Ceramics International

Computational modelling of the effect of microstructure on the abrasive wear resistance of tungsten-carbide nickel composite coatings under sub-critical cyclic impact loading

--Manuscript Draft--

Manuscript Number:	
Article Type:	Full length article
Keywords:	Abrasive wear; Finite element modelling; Material removal mechanism; Metal matrix composite coating (MMC)
Corresponding Author:	Mohammad Parsazadeh, Ph.D. University of Alberta Edmonton, Alberta CANADA
First Author:	Mohammad Parsazadeh, Ph.D.
Order of Authors:	Mohammad Parsazadeh, Ph.D.
	Gary Fisher, PhD
	Andr´e McDonald, PhD
	James D. Hogan, PhD
Abstract:	Abrasive wear was simulated for tungsten carbide-nickel (WC-Ni) composite coatings with different volume fractions of reinforcing particles under abrasive cyclic loading. Using parallelized computing approaches, for the first time in the literature, the effects of reinforcing particles and normal load on material removal mechanisms and wear rates were numerically analyzed for multi-cycle loading. The results demonstrated how various material removal mechanisms compete with each other for varying load, cycles, and particle concentrations. This both confirmed previous experimental observations, as well as motivates future areas towards materials tailoring and optimization. Finally, a statistical predictive model was developed to define the relationship between the wear rate, reinforcing particles volume fraction, and load in order to inform future efforts in materials design.
Suggested Reviewers:	Richard Chromik, PhD McGill University richard.chromik@mcgill.ca Expert in this field
	Sanjay Sampath, PhD Stony Brook University ssampath@ms.cc.sunysb.edu Expert in this field
	Adrian Gerlich, PhD University of Waterloo agerlich@uwaterloo.ca Exper in this field.
	Fardad Azarmi, PhD Northern State University fardad.azarmi@ndsu.edu Expert in this field
	Kantesh Balani, PhD Indian Institute of Technology Kanpur kbalani@iitk.ac.in Expert in this field
Opposed Reviewers:	

Computational modelling of the effect of microstructure on the abrasive wear resistance of tungsten-carbide nickel composite coatings under sub-critical cyclic impact loading

Mohammad Parsazadeh[a,*], Gary Fisher[b], André McDonald[a], James D. Hogan[a]

[a] *Department of Mechanical Engineering, University of Alberta, Edmonton, AB T6G 2R3, Canada*
[b] *InnoTech Alberta, Edmonton, Alberta, T6N 1E4, Canada*

Abstract

Abrasive wear was simulated for tungsten carbide-nickel (WC-Ni) composite coatings with different volume fractions of reinforcing particles under abrasive cyclic loading. Using parallelized computing approaches, for the first time in the literature, the effects of reinforcing particles and normal load on material removal mechanisms and wear rates were numerically analyzed for multi-cycle loading. The results demonstrated how various material removal mechanisms compete with each other for varying load, cycles, and particle concentrations. This both confirmed previous experimental observations, as well as motivates future areas towards materials tailoring and optimization. Finally, a statistical predictive model was developed to define the relationship between the wear rate, reinforcing particles volume fraction, and load in order to inform future efforts in materials design.

Keywords: Abrasive wear, Finite element modelling, Material removal mechanism, Metal matrix composite coating (MMC).

*Corresponding author
Email address: parsazad@ualberta.ca (Mohammad Parsazadeh)

1. Introduction

Metal matrix composite (MMC) coatings and overlays have attracted significant attention from industrial and scientific communities due to their unique combination of hardness, strength, and toughness [1, 2], with flexibility towards tailoring metal and reinforcement properties and geometries towards optimized and improved performance [3]. In MMC coatings and overlays, a wide range of carbide particles have been used to date to reinforce the matrix, such as SiC [4], TiC [5], and B_4C [6]. Among these MMC coatings and overlays used in different applications, tungsten carbide (WC)-based MMC coatings and overlays are attractive choices due to their unique combination of hardness and fracture toughness [1]. The combination of WC with Ni-based alloys effectively improves resistance against wear and abrasive damage [7–9], and is especially favorable in manufacturing industries [10] and petroleum [11] applications.

Under abrasive wear, material removal mechanisms may change and evolve when probing the response of single or multiphase materials [12]. For example, these material removal mechanisms include microploughing [13], microcutting [14], microcracking [15], and microfatigue [16]. In single scratch loading, the abrasive wear mechanism is strongly related to angularity of the abrasive particle [17], as well as other intrinsic and external factors, such as temperature, normal load and velocity, microstructure, volume fraction, morphology, and particle size [18–23]. In the study by Varga *et al.,* [19], the dominant material removal mechanism of a Ni-based material with a carbide network was observed to change with changing the loads and temperature. In another study by Parsazadeh *et al.,* [21], the material removal mechanism is likely to change from microploughing to microcutting with increasing volume fraction of the reinforcing particles at high loads. Finally, it is also known that the wear rate varies significantly with changes of abrasive size and shape; however, the relationship between the predominant wear mechanism and the size and shape of the abrasive body is not necessarily straightforward [24]. In this study, we seek to unravel the effects of reinforcing particle volume fraction and load on the abrasive response of nickel-based composite coatings, which could also be applied to reasonably thick overlays.

In the literature, numerical modelling has been used to better understand the impact of different parameters on the material removal mechanisms and wear rate. The stress distribution in fine-carbide grain size coatings [23] and the effects of carbide size and mean free path on composite deformation [25] were evaluated previously with two-dimensional numerical models. For example, a two-dimensional numerical model was developed by Hu *et al.,* [26] to evaluate the effects of the size and volume fraction of WC particles on scratch resistance in WC-Ni composites. The same authors [27] developed a two-dimensional numerical model to analyze the effect of various parameters on material removal, such as WC particle shape, distribution of reinforcement, and their interaction on the material removal. In their study, Melendez *et al.,* [1] used an empirical model to predict wear rate, but was unable to properly predict wear rates without introducing experimental data. Parsazadeh *et al.,* [21] developed Johnson-Cook and Johnson-Holmquist models to predict the mechanical behavior of Ni and WC phases, respectively, but not the interplay of changing material removal mechanisms on predictive modelling of the wear rate of Ni-reinforced composites.

In the literature, the effect of increasing the number of loading cycles has also been explored. For example, Kato [28] experimentally evaluated the abrasive wear and competition of material removal mechanisms in steel at 10 sliding cycles and found that if the sliding is repeated on the same groove, the dominant material removal mechanism changes with increasing number of cycles at large loads (e.g., $\geq$ 0.7 N), while microploughing was the only material removal mechanism in all cycles at low loads (e.g., 0.07 N). In a similar study, Kitsunai *et al.,* [29] studied the material removal mechanisms during low-cycle fatigue of SUS 304 stainless steel using a scanning electron microscope tribosystem and reported that the changes in the material removal mechanisms are sensitive to the normal load and penetration depth. In a separate study by Mezlini *et al.,* [30], the wear resistance of 5xxx aluminium alloys concluded that changes in dominant failure mechanisms are strongly related to the indenter geometry and behaviour of the material in the early sliding cycles. Despite some advances in experimental approaches used to evaluate abrasive wear under cyclic loading [28, 29], no numerical model has been developed to date to evaluate the material removal mechanisms under cyclic sliding wear. This will be addressed in this study, where efforts will be made to better understand interaction in mechanisms activated during cyclic sliding wear in MMC coatings. Specifically, in this article, the effect of normal load and reinforcing particle volume fraction on the abrasive wear resistance of tungsten-carbide nickel (WC-Ni) composite coatings under sub-critical cyclic loading was computationally analyzed for the first time in the literature. The results of this study could also be applied to reasonably thick WC-Ni composite overlays. Following validation with experimental cyclical abrasive data from the literature [31], the model was then evaluated for different load and particle concentration to explore their effect on wear removal mechanisms. Following this, a wear mode diagram was developed to map the dominant material removal mechanism at each cycle at different loads. Using the numerical data, a statistical model was developed to predict the wear rate based on the volume fraction of the reinforcement particles and load.

2. Model and theory

2.1. Physical model

To evaluate the effects of reinforcing particle volume fraction and load on the material removal mechanisms during abrasive wear in nickel-tungsten carbide coating, a three-dimensional model for cyclic sliding wear was developed. The abrasive particle size was selected as 140 μm based on previous studies [32], and the geometry dimensions of the simulation were selected $1\times0.6\times0.25$ mm^3 (Fig. 1, discussed in next section). The geometry size was selected based on the guidelines introduced by Bucaille *et al.,*[33] and Tabor [34], who discussed that the geometry thickness must be four times greater than the scratch depth, and also the geometry width must be ten times greater than the scratch width. The matrix and the reinforcing particles were considered as nickel (Ni) and tungsten carbide (WC), respectively due to the unique combination of hardness and fracture toughness [21]. To evaluate the effect of the reinforcing particles volume fraction and applied load on the dominant material removal mechanism and wear rate, three different volume fractions (ϕ = 10 vol.%, 30 vol.%, and 50 vol.%) and three different loads (P = 100 mN, 300 mN, and 500 mN) were chosen. The reinforcing particles size was considered as 60 μm, which was motivated by experiments [1]. To evaluate the wear rate mechanisms and abrasive wear under subcritical cyclic loading, the loading range was chosen based on the experimental data of Kato [28] and Kitsunai *et al.,* [29].

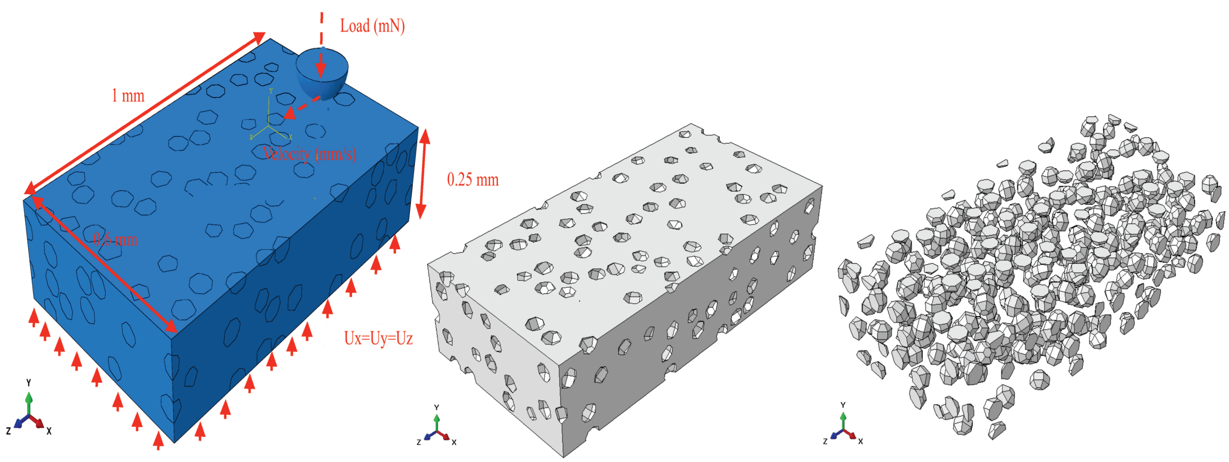

(a) (b) (c)

Figure 1: Schematic diagram of (a) the abrasive particle and the composite coating, (b) the Ni matrix, and (c) WC particles contained with the matrix material.

2.2. Finite element modelling

Abaqus software was used to develop a finite element model, describing the single particle abrasion process. The 140 μm diameter abrasive particle was considered as rigid, and it was used to apply a load at the center of the simulation geometry (Fig. 1a). A surface-to-surface contact [35] was considered between the abrasive particle and both matrix (Fig. 1b) and reinforcing particles (Fig. 1c). The interaction of the matrix and reinforcing particles was defined by a general contact algorithm, which has been used by other authors [21, 36]. Perfect bonding was assumed between the reinforcing particles and the matrix with consideration of the metallurgical bonding observed in the plasma-transferred arc (PTA) fabrication method [37] that is used to fabricate the coatings in the real-world application of the results from the current study.

The abrasive particle was considered under a normal load pushing the particle toward the substrate in the y-direction, while the abrasive particle moves along the z-direction with a speed of 100 mm/s based on Gao *et al.,* [38] and Guo *et al.,* [39] studies. A mesh independency study was conducted, and a minimum of 50,000 elements was chosen in this study to keep the results independent of the number of elements. The bottom surface of the substrate was constrained in all directions. Each cycle of the sliding simulation was completed in four steps. In the first step, a contact was established between the abrasive particle and the substrate by gradually increasing the normal load until the load reached its maximum at the end of the step. In the second step, the abrasive particles moved along the z- direction with a constant velocity. In the third step, the particle moved backward with the same speed and load as step 2 until it reached its origin point. In the last step, the abrasive particle was unloaded by gradually lifting it up. This procedure was repeated for ten cycles to evaluate the effect of the number of cycles on the material removal mechanisms. The effect of the number of cycle on the material removal was also evaluated for ten cycles in the experiments performed by Kitsunai *et al.,*[29] on SUS 304 stainless steel and by Kato *et al.,* [28] on steel. Abaqus Explicit was used to simulate the plastic deformation and material removal of the WC-Ni coating. The element type chosen to mesh the substrate was a ten-node quadratic tetrahedron (C3D10 in ABAQUS FEA notation), while the abrasive particle was meshed using 3-node 3-D rigid triangular facets (R3D3 in ABAQUS FEA notation). These types of mesh were also used by Rolland *et al.,* [40] and Pal *et al.,* [41]. To perform high-powered parallel computing and reduce the computation time, Compute Canada clusters were employed and paralleled, with a typical run time of 40 h per simulation on two nodes.

2.3. Constitutive models

To model plastic and damage behaviour of the Ni matrix during abrasive loading, the Johnson-Cook (J-C) constitutive equation [42] was used. In the J-C model, the relationship between von Mises flow stress σ_{eq}, yield stress, hardening, and temperature softening is expressed as:

$$\sigma_{eq} = [A + B\bar{\epsilon}^{pl})^N][1 + Cln(\frac{\dot{\bar{\epsilon}}^{pl}}{\dot{\bar{\epsilon}}_0^{pl}})][1 - (\frac{T - T_{ref}}{T_{melt} - T_{ref}})^M] \tag{1}$$

where A is the yield strength, B is the strain-hardening modulus, $\bar{\epsilon}^{pl}$is the equivalent plastic strain, C is the strain rate hardening coefficient, $\dot{\bar{\epsilon}}^{pl}$is the equivalent plastic strain rate, $\dot{\bar{\epsilon}}_0^{pl}$ is the reference strain rate, T is the temperature at the operating condition, T_{ref} is the reference temperature, T_{melt} is the melting temperature, and N and M are the strain hardening exponent and softening exponent, respectively.

Based on the equivalent plastic strain $\Delta\epsilon^{pl}$, a damage parameter (D) is defined in the J-C damage model as:

$$D = \sum \frac{\Delta\epsilon^{pl}}{\epsilon_f^{pl}} \tag{2}$$

where ϵ_f^{pl} is equivalent plastic strain at failure, which is defined as:

$$\epsilon_f^{pl} = [D_1 + D_2 exp(D_3(\frac{\sigma_m}{\sigma_{eq}}))][1 + D_4 ln(\frac{\dot{\epsilon}^{pl}}{\dot{\epsilon}_0^{pl}})[1 + D_5(\frac{T - T_{ref}}{T_{melt} - T_{ref}})] \tag{3}$$

where D_1 to D_5 are material constants and σ_m is the mean stress.

To simulate the response of WC particles during deformation, the Johnson-Holmquist (JH-2) constitutive model was employed [43]. In this model, the strength of the material is related to pressure, strain rate, and damage accumulation. Initially, elastic deformation is considered in the material, and the stress-state is described based on the elastic material properties and equation of state. Based on the material deformation, the relationship between pressure on the material density is expressed as:

$$P = K_1\mu + K_2\mu^2 + K_3\mu^3 \ \ if \ \ \mu \geq 0 \tag{4}$$

$$P = K_1\mu \ \ if \ \ \mu \leq 0 \tag{5}$$

where $\mu = \rho/\rho_0$, ρ is the material density, ρ_0 is the reference density, and K_1, K_2, and K_3 are constants.

In the Johnson-Holmquist model, an increment in damage causes material bulking, and this means that fractured material occupies larger volume when compared to the intact condition, which leads to an increase in local pressure in a constrained material. The bulking pressure is zero at the initial step for an undamaged material, and the bulking pressure is calculated at the next time step as [44, 45]:

$$\Delta P_{t+\Delta T} = -K_1\mu_{t+\Delta t} + [(K_1\mu_{t+\Delta t} + \Delta P_t)^2 + 2\beta K_1 \Delta U]^{1/2}, \tag{6}$$

where β is the fraction of elastic energy loss converted to potential hydrostatic energy and ΔU is the energy loss due to increased bulking pressure, which is defined as [46]:

$$\Delta U = U(D) - U(D_{n+1}) \tag{7}$$

where $U(D) = \frac{\sigma}{6G}$, and G is the elastic shear modulus.

In the JH-2 model, damage accumulates progressively with plastic deformation under loading. To track the damage accumulation, a damage parameter, varying from 0 to 1 is employed. The overall material strength degradation is also based on this damage parameter. The strength of the material is defined in terms of the normalized von Mises equivalent stress as [45]:

$$\sigma^* = \sigma_i^* - D(\sigma_i^* - \sigma_f^*), \tag{8}$$

where D is the damage parameter, and σ_i^* and σ_f^* are the normalized intact and fractured equivalent stresses, respectively. The normalized equivalent stresses have the general form of $\sigma^* = \sigma/\sigma_{HEL}$. In this definition, σ is the von Mises equivalent stress and σ_{HEL} is the equivalent stress at the Hugoniot elastic limit (HEL).

In the JH-2 model, the evolution of the damage is similar to those in the J-C model described in Eq. (2). However, the fracture strain definition is given as the following in the JH-2 model:

$$\epsilon pl_f = D_1(P^* + T^*)^{D_2}, \tag{9}$$

where D_1 and D_2 are damage constants, which describe the relationship between fracture strain, normalized pressure, and normalized maximum tensile hydrostatic pressure for a particular material.

In the JH-2 model, the normalized intact stress is defined as a function of pressure and strain rate as:

$$\sigma_i^* = A(P^* + T^*)^N(1 + Cln\dot{\epsilon}^*) \tag{10}$$

130 where A and C are material constants, and T^* is the normalized maximum tensile hydrostatic pressure.

Similarly, the fractured stress is defined as:

$$\sigma_f^* = B(P^*)^M(1 + Cln\dot{\epsilon}^*), \tag{11}$$

where B, M, and N are material constants, P^* is the normalized pressure, which is expressed as:

$$P^* = P/P_{HEL} \tag{12}$$

and T^* is expressed as:

$$T^* = T/P_{HEL}, \tag{13}$$

where P_{HEL} is the pressure at the HEL and T is the maximum tensile pressure that a material can withstand. HEL experimental data is needed to determine P_{HEL} and σ_{HEL}. The HEL represents the point at which the shock wave exceeds the elastic limit of the material and is presented as a one-dimensional shock wave [45]. The HEL is defined as:

$$HEL = P_{HEL} + \frac{2}{3}\sigma_{HEL}. \tag{14}$$

Eq. (14) is used to find the values of P_{HEL} and σ_{HEL} using a procedure described in many studies where the JH-2 model was implemented [44, 45, 47]. Correspondingly, the volumetric strain at the HEL is calculated as [45]:

$$HEL = K_1\mu_{HEL} + K_2\mu_{HEL}^2 + K_3\mu_{HEL}^3 + \frac{4}{3}G\frac{\mu_{HEL}}{1 + \mu_{HEL}}. \tag{15}$$

The material parameters used in the J-C and JH-2 models are listed in Table 1 for Ni and WC. The Ni properties were obtained from Ghelichi *et al.,* [48], and WC properties given by Moxnes *et al.,*[49] and Holmquist *et al.,*[50] were used in this study.

Table 1: Properties and constants used in J-C and JH-2 constitutive models for Ni and WC.

Material properties	Ni [48]	WC
A	163 [MPa]	0.9899 [49]
B	648 [MPa]	0.67 [49]
C	0.06	0
E	200 [GPa]	N/A
M	1.44	0.0322 [49]
N	0.33	0.0322 [49]
$\dot{\bar{\epsilon}}_0^{pl}$	1	1
ρ_0 [kg/m^3]	8900	14560
υ	0.31	N/A
D_1	0.54	0.005[49]
D_2	4.89	1 [49]
D_3	3.03	N/A
D_4	0.014	N/A
D_5	1.12	N/A
G [GPa]	N/A	219 [49]
HEL [GPa]	N/A	6.566 [49]
IDamage	N/A	0
K_1 [GPa]	N/A	362 [50]
K_2 [GPa]	N/A	694 [50]
K_3 [GPa]	N/A	0 [50]

3. Results and discussion

To validate the FE model developed in this study with experimental data, the results of this study were first compared with experimental WC-Ni scratch test results of Alzouma *et al.,* [51]. The displacement contour of the current numerical model is shown in Fig. 2(a). Based on the materials used in the Alzouma *et al.,* [51] study, a volume fraction of 6.8 vol.%, abrasive particle size of 400 μm, and normal load of 15 N were chosen. As the microstructure of the composite coating studied by the Alzouma *et al.,* [51] could have spatially varying microstructure and results, three scratch profiles (noted in Fig 2.a) were extracted at different locations from the current study and compared with the scratch profile obtained by Alzouma *et al.,* [51]. The position in the x-direction is divided by the width of the sample to obtain the dimensionless wear width for easier comparison, as shown in Fig. 2 (b). The scratch profile obtained from the FE model can reasonably predict the scratch profile obtained experimentally. A slight difference between the current scratch profiles and those obtained experimentally could be attributed to the small differences in the distribution and size range of the WC particles, which were not explicitly reported by Alzouma *et al.,* [51] but assumed here based on micrograph images from their study, Additional differences may arise from the chosen location of the profile measurement, which were not explicitly detailed in the Alzouma *et al.,* [51] study.

To further validate the current FE model with experimental data, an FE model, simulating the multi-cycle abrasive wear of WC-Ni composite coatings was developed using the operating conditions reported by Alidokht *et al.,* [31]. To account for slightly unknown values of volume fraction, particle size, and exact load settings in the study by Alidokht *et al.,* [31], these values were allowed to vary in the simulation by $\pm$ 30%. The simulation results for the wear rates obtained after 10 cycles and compared with the experimental results [31] are shown in Fig. 2 (c). The lower bound represents $\phi = 7$ vol.%, the middle cross represents the average, and the lower cross represents $\phi = 13$ vol.%. The wear rate range obtained using the current FE model can predict the experimental data by Alidokht *et al.,* [31] with average deviation of 17%.

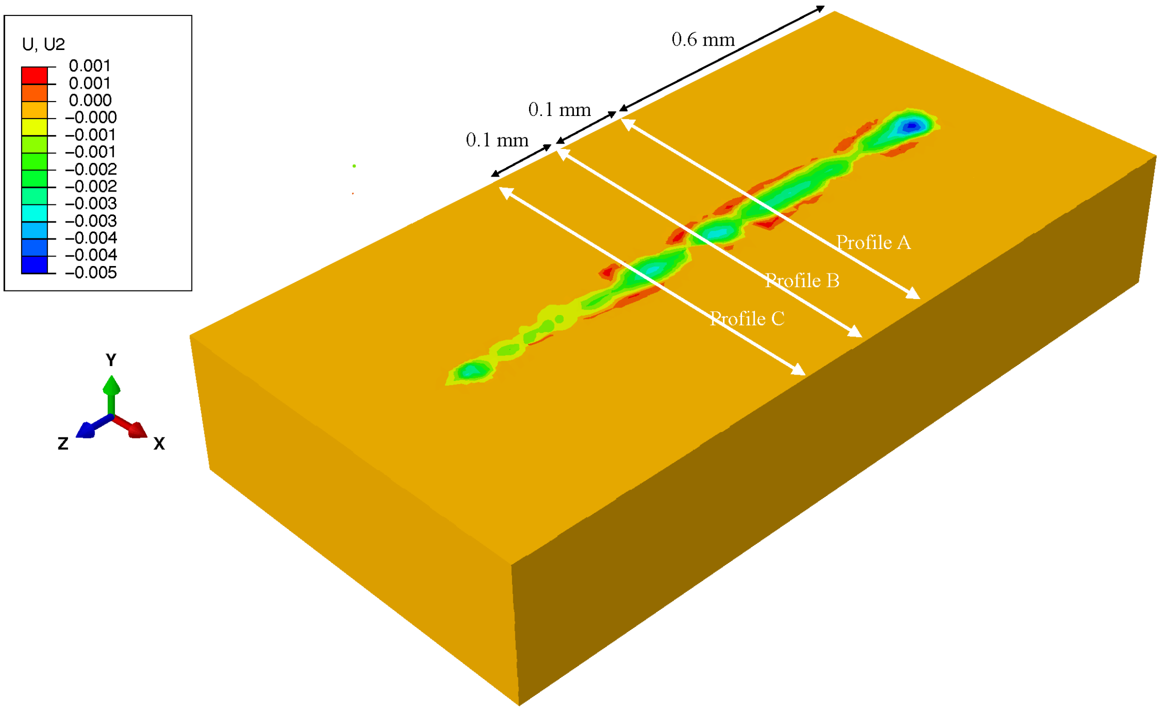
U, U2
0.001
0.001
0.000
−0.000
−0.001
−0.001
−0.002
−0.002
−0.003
−0.003
−0.004
−0.004
−0.005
0.6 mm
0.1 mm
0.1 mm
Profile A
Profile B
Profile C
Y
Z
X

(a)

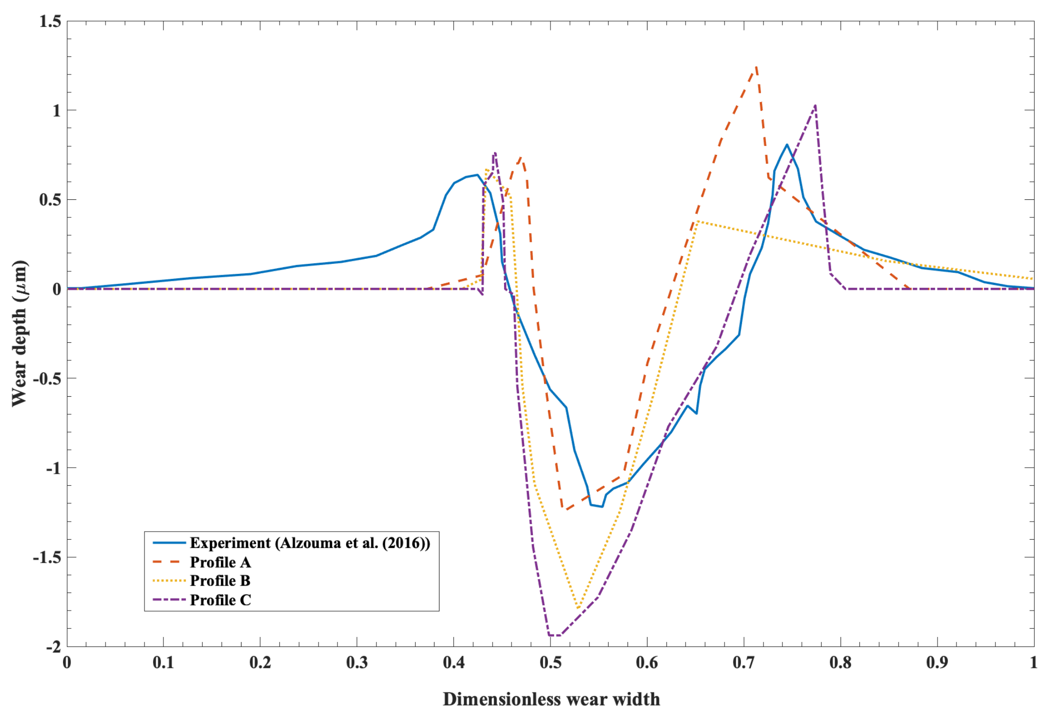
Wear depth (μm)
Dimensionless wear width
Experiment (Alzouma et al. (2016))
Profile A
Profile B
Profile C
1.5
1
0.5
0
-0.5
-1
-1.5
-2
0
0.1
0.2
0.3
0.4
0.5
0.6
0.7
0.8
0.9
1

(b)

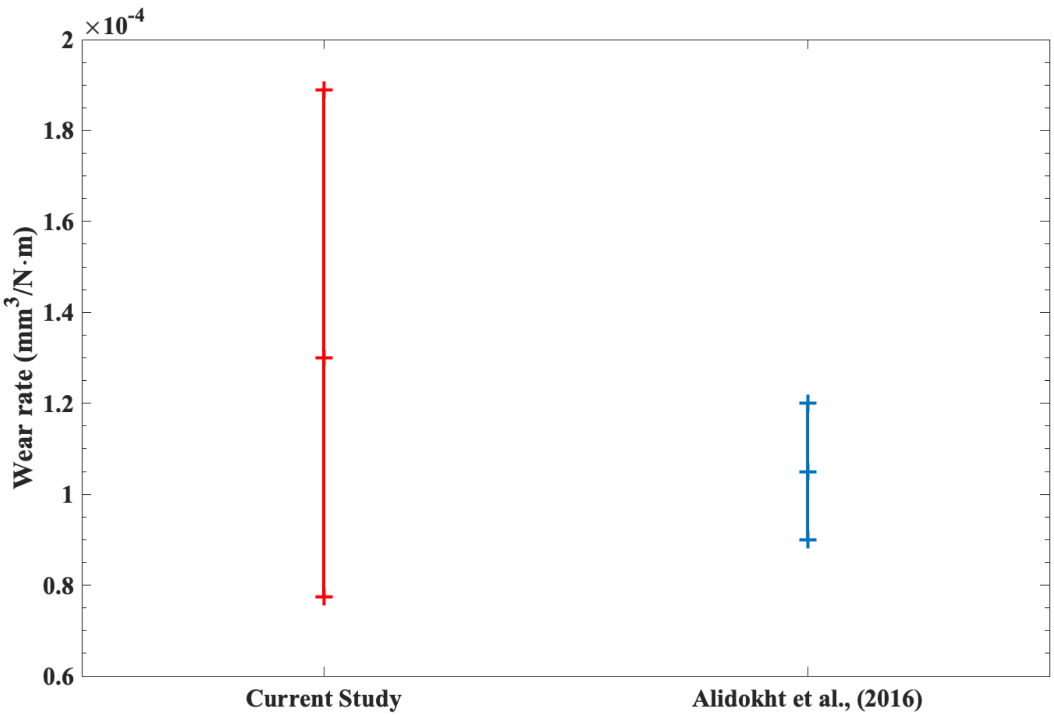

(c)

Figure 2: (a) Profile locations in the WC-Ni coating used for the numerical and experimental comparisons, (b) comparison of scratch profiles of WC-Ni coating from the present model and the experimental data from Alzouma *et al.,* [51], and (c) the wear rate comparison of the current study with the Alidokhot *et al.,*[31] experimental study.

3.1. Simulation of residual stress and displacement

Next, we explore the spatial distribution of deformation in the material by investigating the spatial distribution of deformation in the material and displacement, the contours of stress and displacement were presented. To evaluate the stress distribution in each MMC coating, von Mises stress contours were used as a parameter describing the plastic flow and fracture, which are the basic causes of the formation of wear asperities [52]. The contours of the residual stress are shown in Fig. 3 for the composite coating with $\phi = 10$ vol.% and $\phi = 50$ vol.% at loads of 100 mN and 500 mN to probe extrema cases of the stress distribution in the substrate after the first cycle, as well as to observe how material removal mechanisms change and evolve as a function of these internal and external parameters and number of cycles. To better compare results across different cases in the plot, the upper limit of the stress range on Fig. 3 was fixed. In the first cycle, no significant material deformation was observed in the cases shown in Fig. 3, and the stress was distributed more uniformly in the case with higher reinforcing particles volume fraction, likely due to a smaller mean free path [53]. Smaller mean free path allows for load sharing across the reinforcing particle phase, which then leads to a more homogeneous distribution of the stress. Also, the stress was mainly concentrated at the interface of the particles and matrix for all of the cases, particularly the ones experiencing higher load, which makes these locations the first to fail [54]. From the literature, this stress concentration at the interface of the particles and matrix has been attributed to the mismatch in the mechanical properties of the matrix and the reinforcing particles [25], and this mismatch in the properties promotes locations for fracture initiation and material removal [21].

Next, the contours of the residual stress are shown at Fig. 4 after 10 cycles. The material has the same particle concentrations and loads as Fig. 3. As expected, the residual stress accumulated more with increasing the number of cycles. No particle removal was observed when the load was 100 mN as shown in Fig. 4 (a, b). At a load of 500 mN, the stress was mainly stored in the form of microfatigue and led to less material deformation with higher particles volume fraction, as shown in Fig. 4 (c, d).

Finally, the displacement contours of the WC-Ni composite coating with $\phi = 10$ vol.% and a load of 500 mN are depicted after cycle 5 in Fig. 5 (a) and after cycle 6 in Fig. 5 (b). The displacement contours were selected for this particular particle volume fraction to analyze the wear rate fluctuations observed for the case with $\phi = 10$ vol.% and for this particular load, as very small particle removal occurred at lower loads. In the 500mN case, the load on the abrasive particle caused the material to plastically deform with no visible particle cracking until cycle 5, as shown in Fig. 5 (a). At cycle 6 (Fig. 5b), the WC reinforcing particles begin to be removed due to the influence of microfatigue on the WC particles. This material deformation behavior and WC particles removal for low cycle abrasion was also observed in the experimental study by Bonny *et al.*, [55].

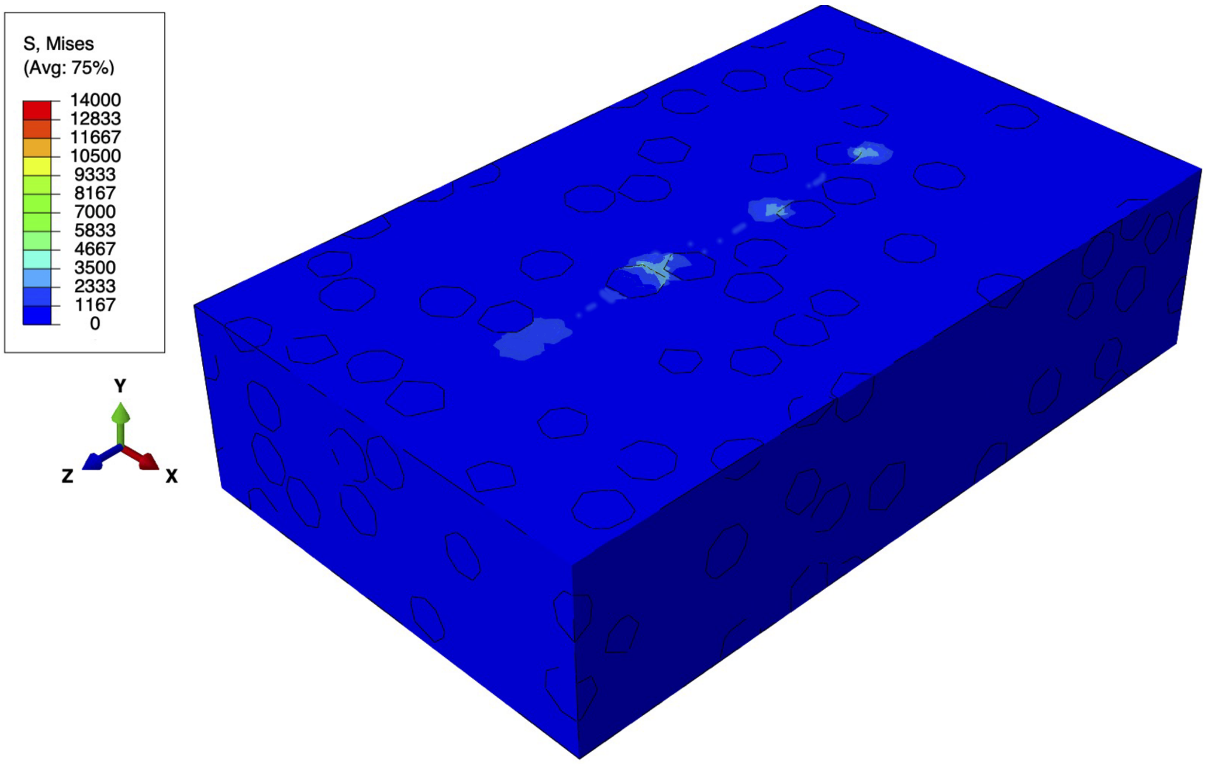
S, Mises
(Avg: 75%)
14000
12833
11667
10500
9333
8167
7000
5833
4667
3500
2333
1167
0
Y
Z
X

(a)

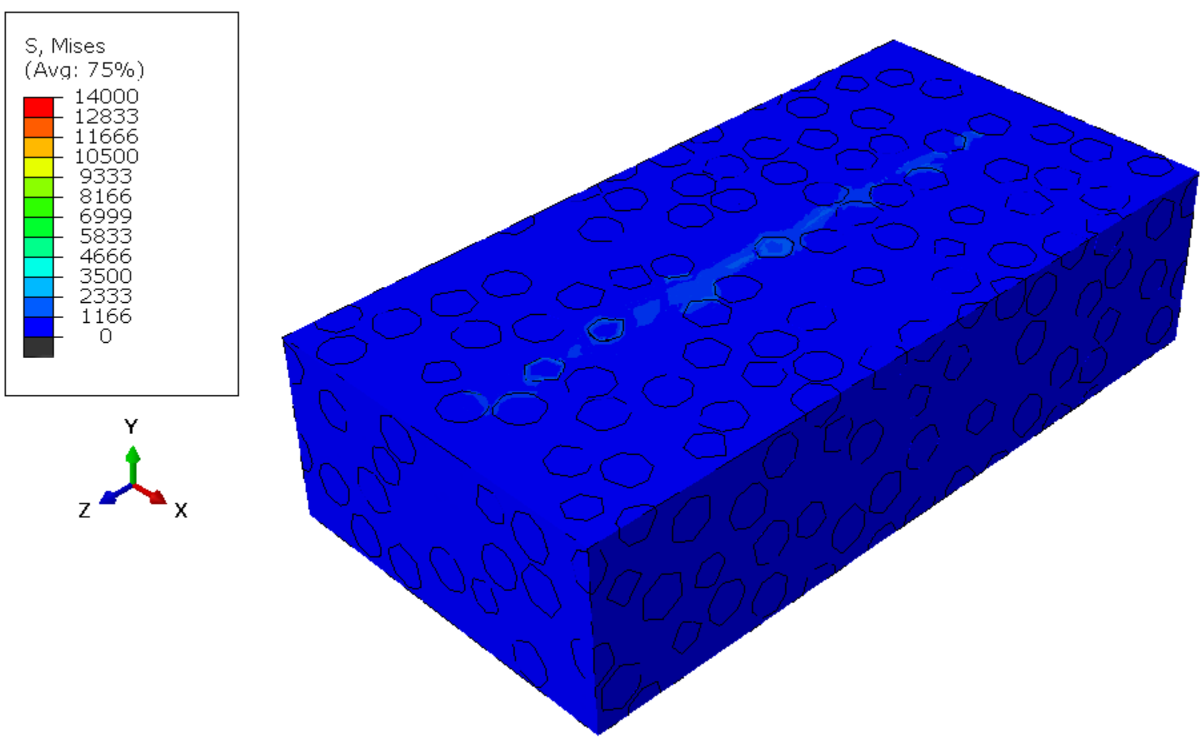
S, Mises
(Avg: 75%)
14000
12833
11666
10500
9333
8166
6999
5833
4666
3500
2333
1166
0
Y
Z
X

(b)

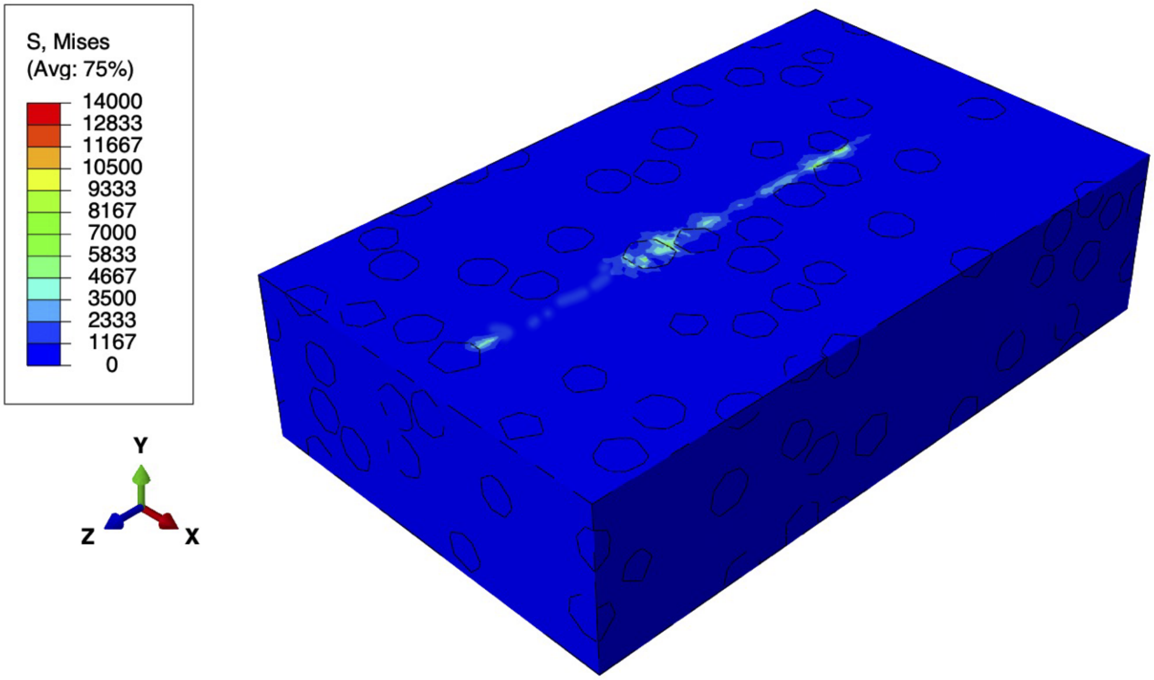

(c)

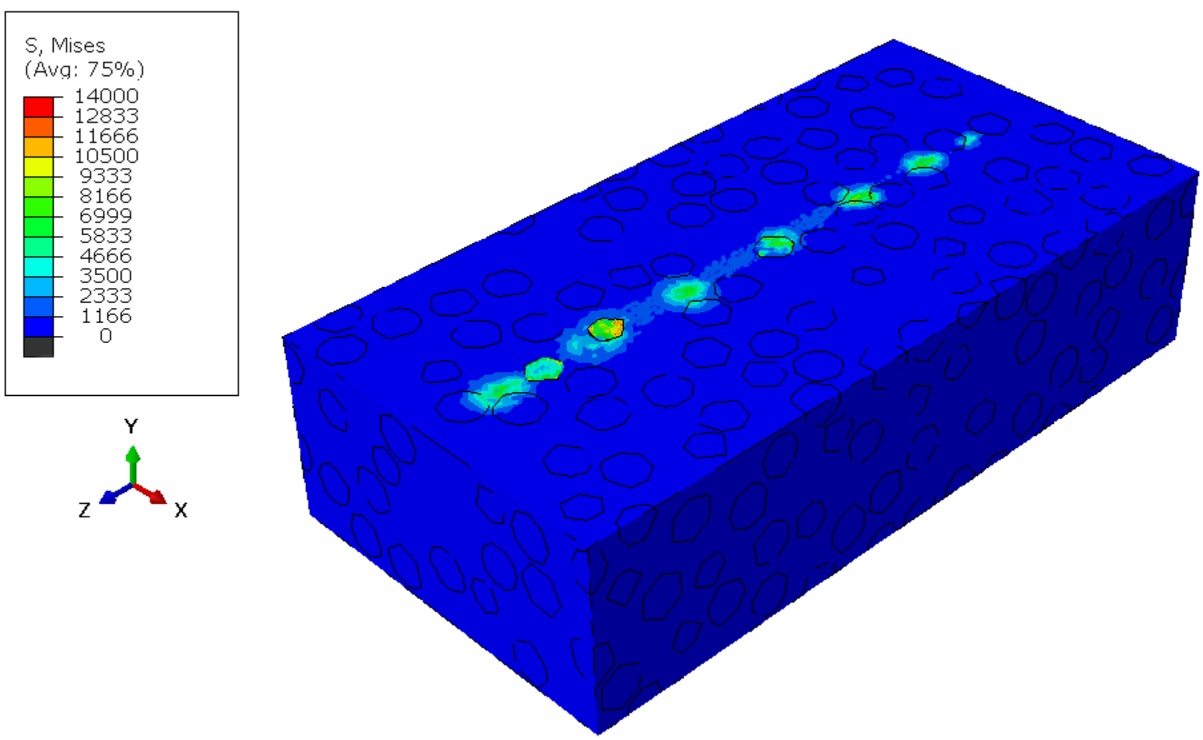

(d)

Figure 3: Residual stress (MPa) shown using von Mises contours after the first cycle for: (a) $\phi = 10$ vol.% and $P = 100$ mN, (b) ϕ=50 vol.% and $P = 100$ mN, and (c) $\phi = 10$ vol.% and $P = 500$ mN (d) $\phi = 50$ vol.% and $P = 500$ mN.

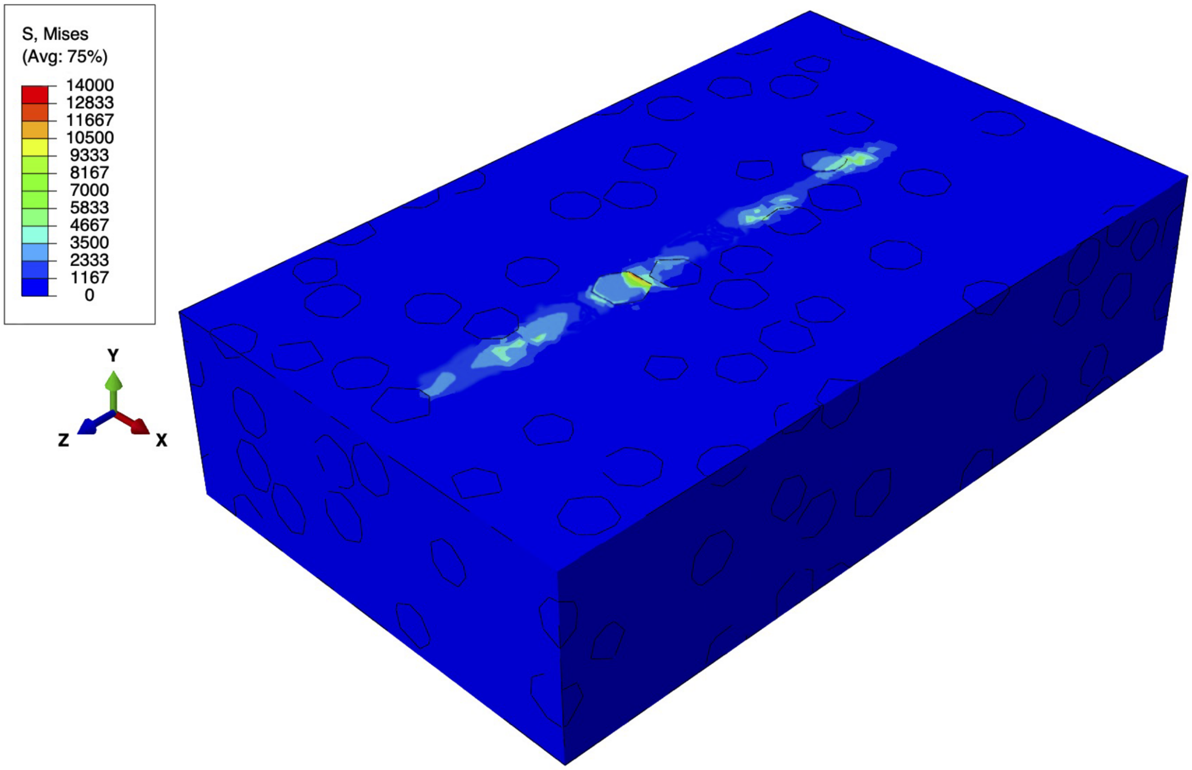
S, Mises
(Avg: 75%)
14000
12833
11667
10500
9333
8167
7000
5833
4667
3500
2333
1167
0
Y
Z
X

(a)

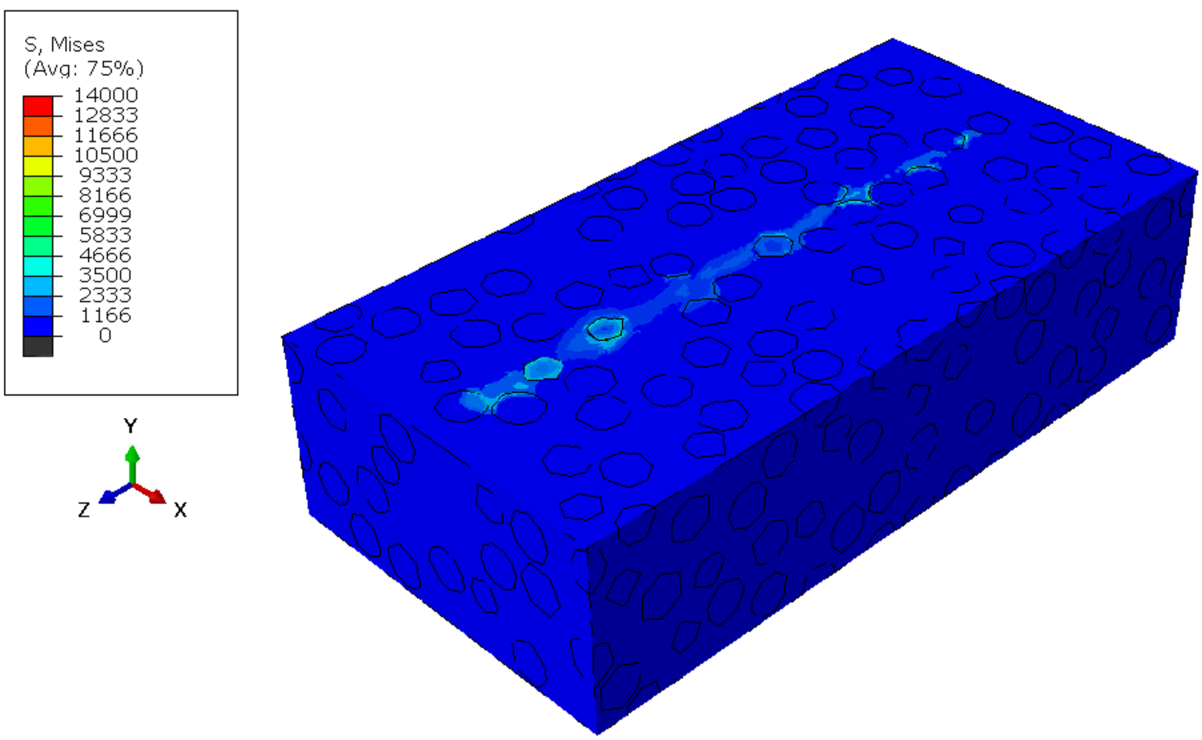
S, Mises
(Avg: 75%)
14000
12833
11666
10500
9333
8166
6999
5833
4666
3500
2333
1166
0
Y
Z
X

(b)

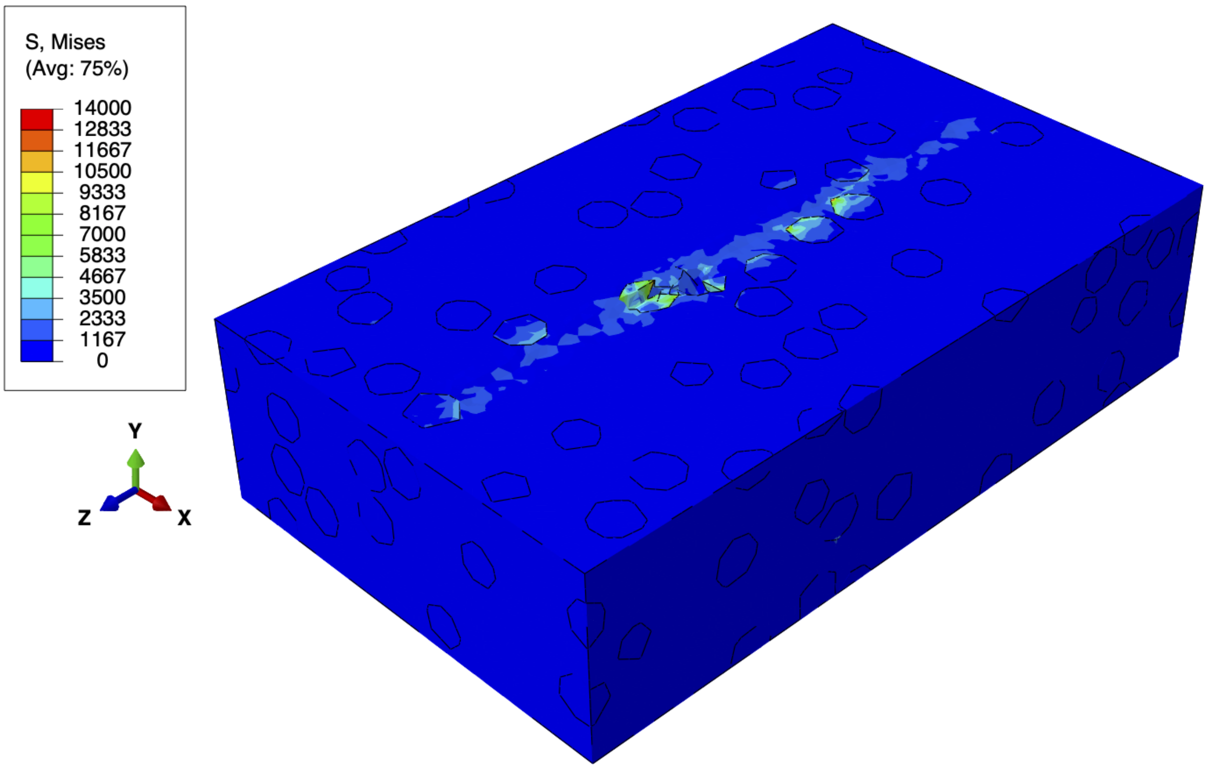

(c)

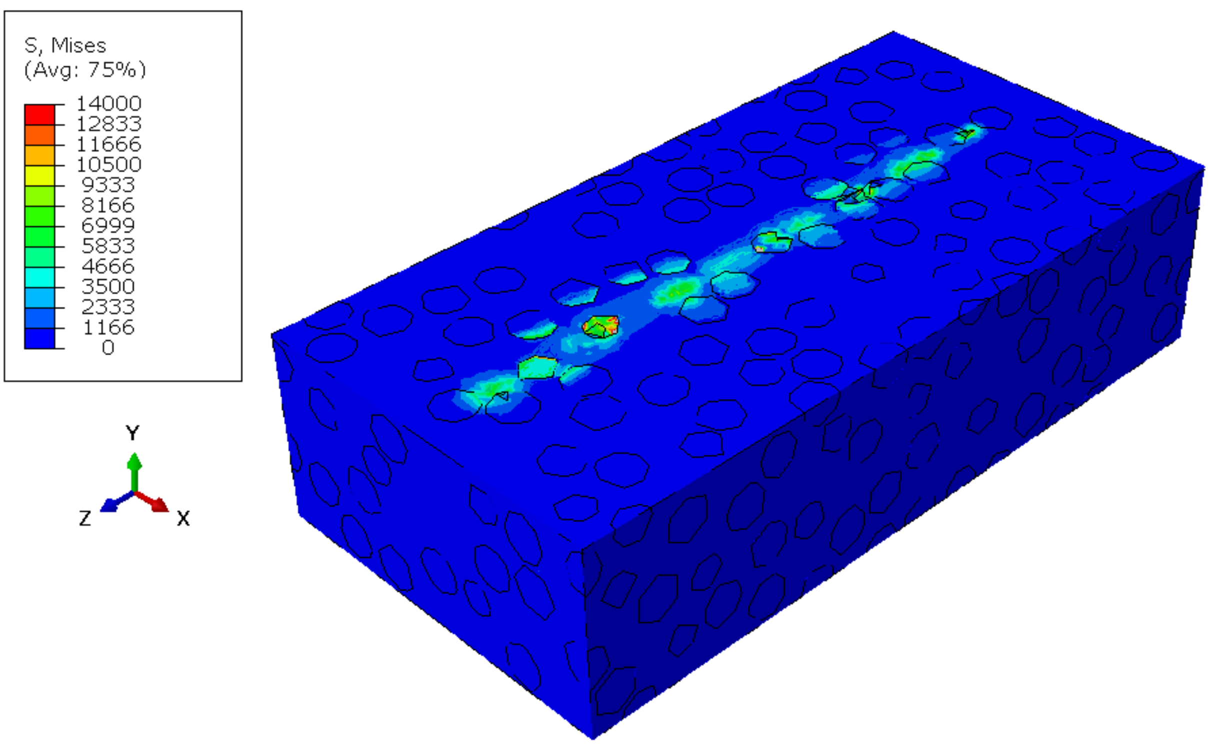

(d)

Figure 4: Residual stress (MPa) shown using von Mises contours after the 10^{th} cycle for: (a) $\phi = 10$ vol.% and $P = 100$ mN, (b) $\phi = 50$ vol.% and $P = 100$ mN, (c) $\phi = 10$ vol.% and $P = 500$ mN, and (d) $\phi = 50$ vol.% and $P = 500$ mN.

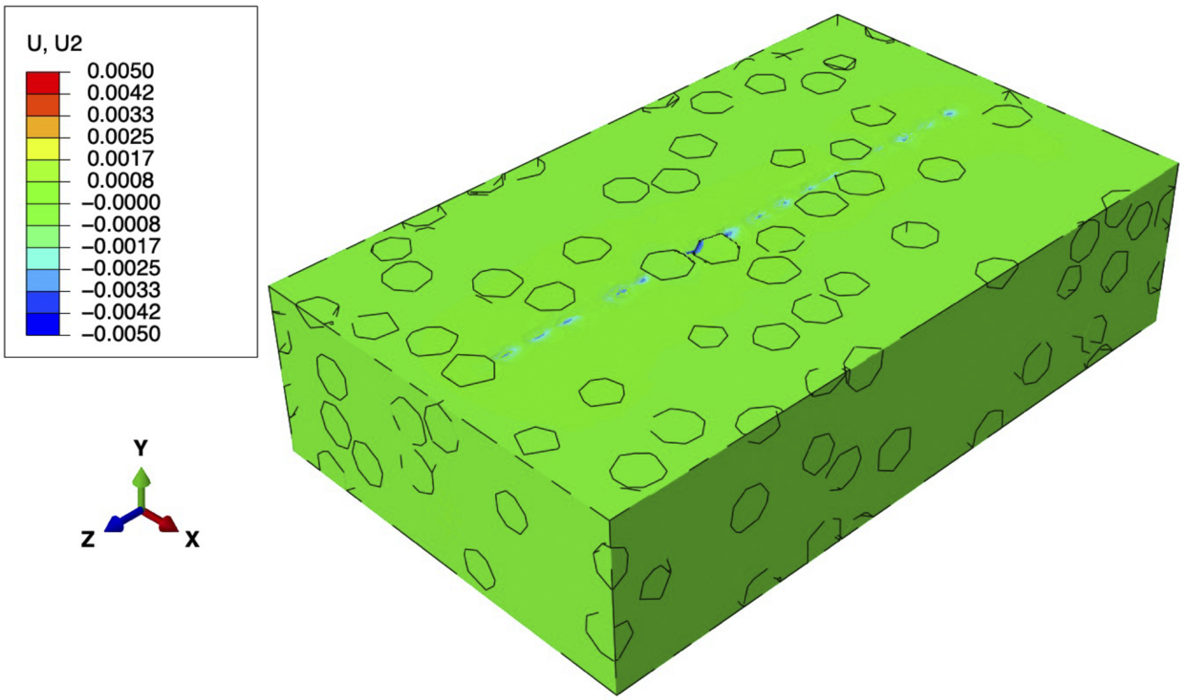

(a)

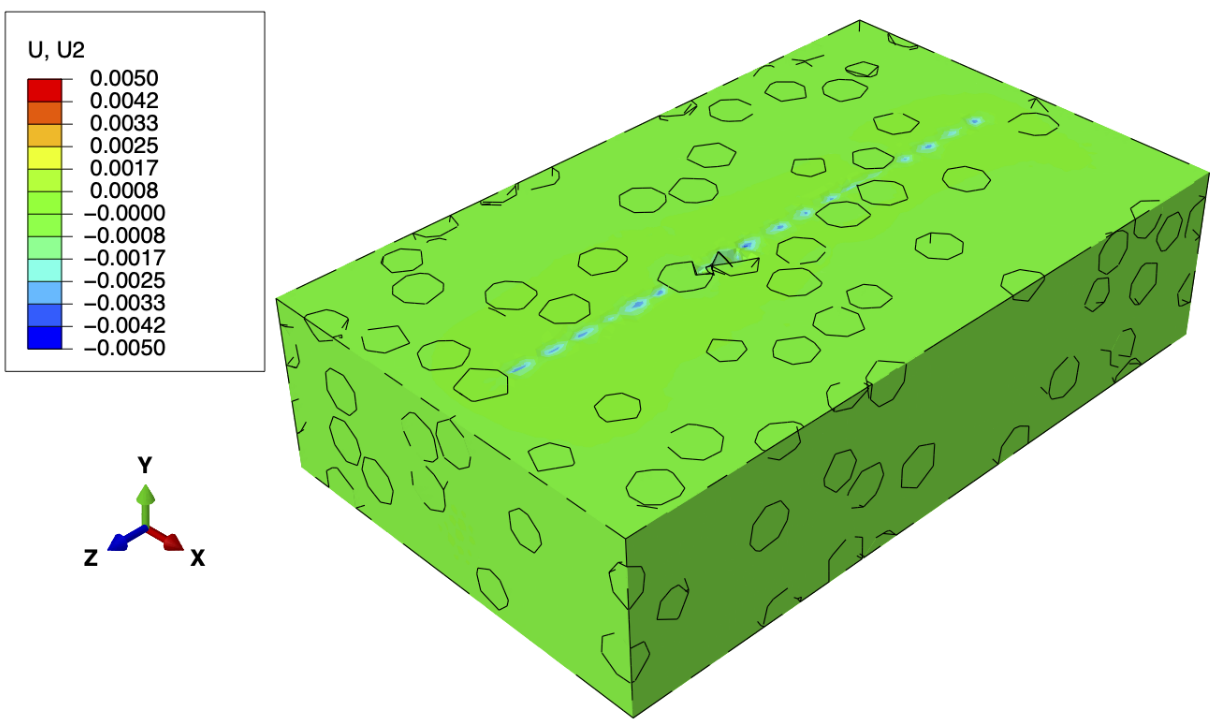

(b)

Figure 5: Displacement (mm) contours of WC-Ni composite coating for $\phi = 10$ vol.% and $P = 500$ mN after cycles of (a) 5 and (b) 6, indicting the initiation of particles cracking.

3.2. Wear rate analysis

We now explore the effect of WC particles volume fraction and load on the resulting wear rate of the material. The wear rate (W) was determined by dividing the volume loss, ΔV, by the applied load and the sliding distance (s) as [1]:

$$W = \frac{\Delta V}{P \cdot s} \tag{16}$$

The wear rate was then determined for each cycle at different loads (P = 100 to 500 mN) and particle volume fraction combinations, as shown in Fig. 6. Regardless of the reinforcing particle volume fraction, the wear rate increased with increasing the load from 100 mN (Fig. 6a) to 300 mN (Fig. 6b), and then to 500 mN (Fig. 6c). At a load of 100 mN, microploughing was the only mechanism of material removal at all cycles, and no reinforcing particles were removed. With increasing the number of cycles, the wear rate of the composite with $\phi = 10\%$ diverged when compared to the composite coating with higher particles volume fractions, as shown in Fig. 6 (a). As noted by the authors in Parsazadeh *et al.,*[21], this could be due to the possible increase in hardness with a trade-off in toughness, smaller mean free path, and better stress distribution of the composite coating with higher particles volume fractions. For the case of 300 mN, the wear rate decreased with increasing particle volume fraction, as shown in Fig. 6 (b). At a load of 500 mN and $\phi = 10$ vol. %, the wear rate slightly fluctuated, as shown in Fig. 6 (c). These fluctuations could have two origins: One, competition of microfatigue with microploughing after the 5^{th} cycle. After additional cycles, the damage parameter in some elements approached 1, which results in no removal of particles and an associated lower wear rate. In the next cycle, those elements with damage close to one begin to be removed, which results in an increase in wear rate. Two, there is a dependency of the wear rate to the path that the abrasive particle has travelled. As the mean free path between the particles is larger at $\phi = 10$ vol. %, the wear rate could be dependent on the number of reinforcing particles that interact with the abrasive particle. The wear rate obtained with higher particles volume fraction was determined to be lower than that of the composite coating with 10 vol. % reinforcing particle, which has been attributed to a lower mean free path [1].

To better understand the wear rate changes at each cycle, the WC particles volume loss was determined at each cycle for all of the cases (ϕ= 10, 30, and 50 vol.%) experiencing loads of 300 mN and 500 mN as shown in Fig. 7. At a load of 300 mN, the WC particles began to be removed after 8 cycles, as shown in Fig. 7 (a), which indicates that fatigue in the reinforcing particles is becoming dominant. As a result of particles being removed, the wear rate increased in all cases when particles are removed (see Fig. 6b). At a load of 500 mN, the lowest wear rate was obtained with 30 vol.% WC particles (see Fig. 6c). For ϕ= 50 vol.% in Fig. 7 (b), the stress concentration increases, and consequently, the particle removal increases at the interface, leading to higher material removal and wear rate.

To summarize the wear mechanisms for each cycle observed during sliding wear of WC-Ni composite coating with volume fractions of 10 vol.% and 50 vol. %, a wear mechanism map was created and this was shown in Fig. 8. A particle volume concentration of 30 vol.% was not chosen because of the limited sensitivity of the change in mechanisms over the studied parameter range. Here, Fig 8(a) and (b) show dominant material removal mechanisms at ϕ = 10 vol. % and ϕ = 50 vol. %, respectively. The color of the points in the figure are chosen to denote whether microploughing or microfatigue is the dominant mechanism. From Fig. 8, we can observe that the wear mechanisms changes with increasing the number of cycles and load. In addition, increasing the reinforcing particles volume fraction results in delaying the onset of microfatigue to appear at later cycles when compared to the composite coating with 10 vol.% of reinforcing particles. This could be a reason for higher wear resistance of the material with WC volume fraction of 50 vol.% than the volume fraction of 10 vol.%. At lower loads, the microploughing was the only mechanism of material removal at each cycle, which was also reported by Kitsunai *et al.,* [29]. The role of microfatigue was observed in the present study dominant at higher loads. It can be concluded that the wear rate decreased with the addition of reinforcing particles, which has also been observed in an experimental study by Melendez *et al.,* [1]. In the Melendez *et al.,* [1], this was due to reduction in the mean free path between the agglomerated WC-based reinforcing particles [1], an increase in the hardness of the coating [27], enhanced resistance to plastic flow of Ni matrix, which was also observed by Alidokht *et al.,*[31].

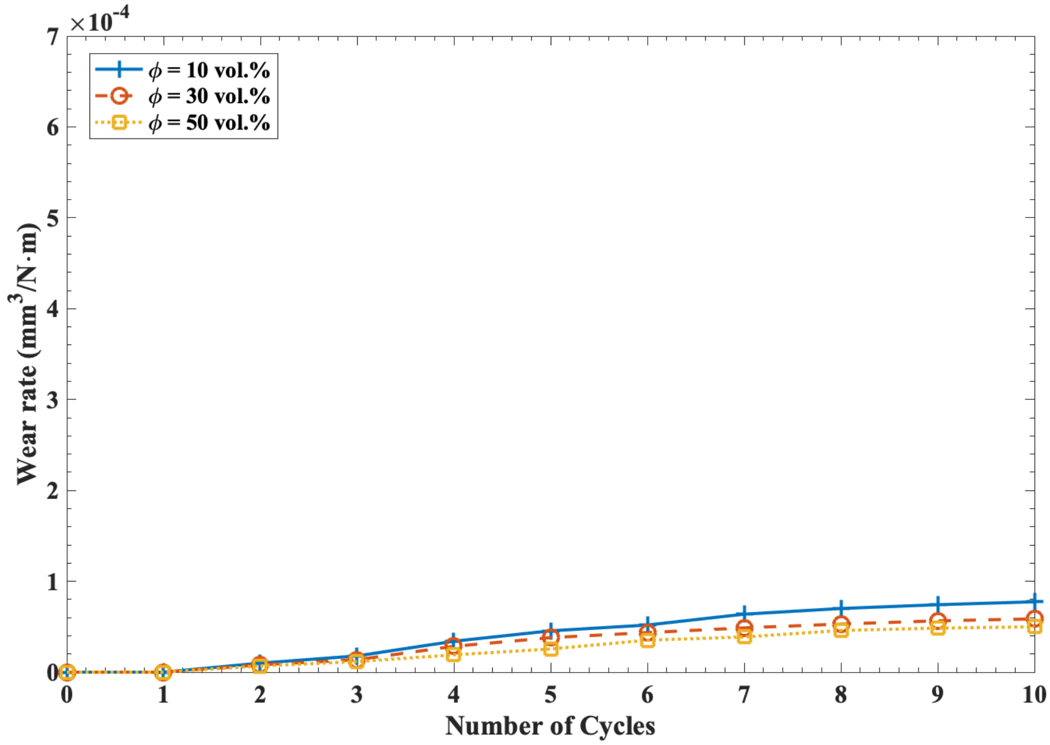
×10^-4
φ = 10 vol.%
φ = 30 vol.%
φ = 50 vol.%
Wear rate (mm^3/N·m)
Number of Cycles
0
1
2
3
4
5
6
7
8
9
10

(a)

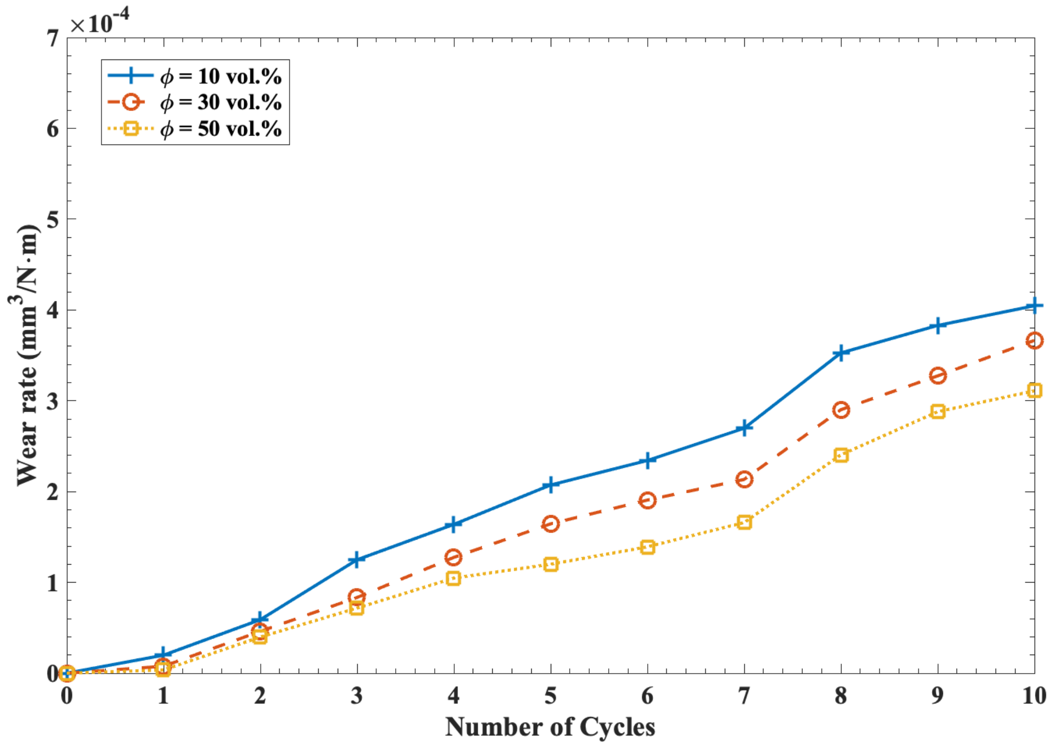
×10^-4
φ = 10 vol.%
φ = 30 vol.%
φ = 50 vol.%
Wear rate (mm^3/N·m)
Number of Cycles
0
1
2
3
4
5
6
7
8
9
10

(b)

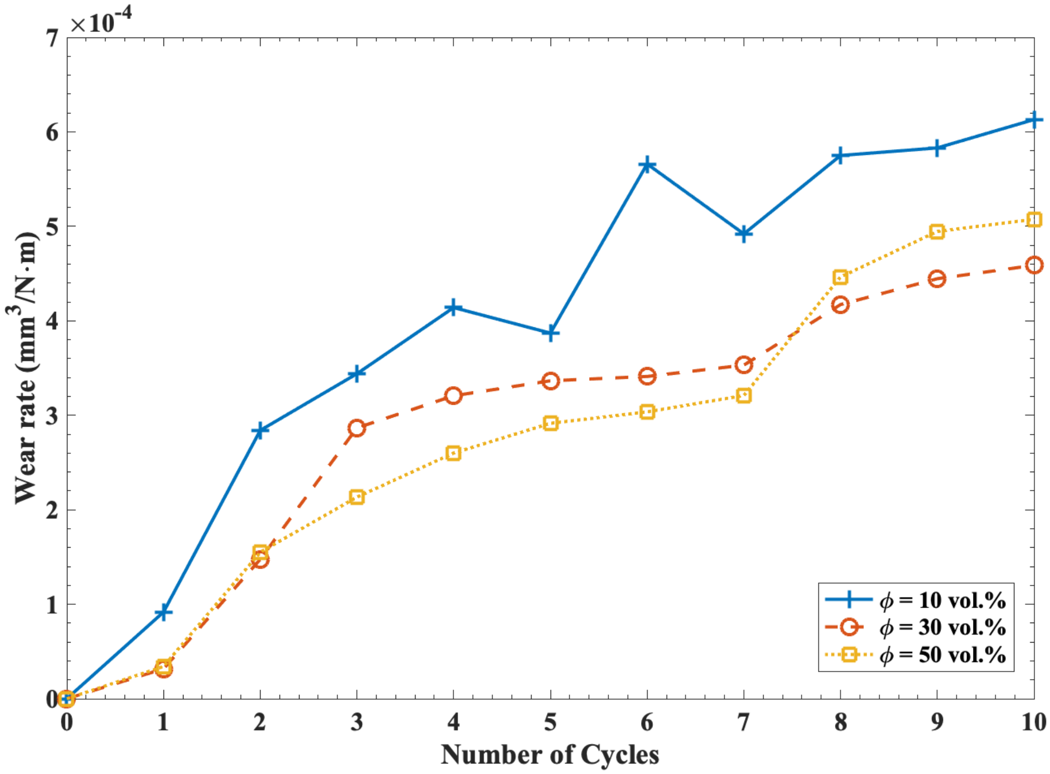

(c)

Figure 6: Wear rate ($mm^3/N \cdot m$) across 10, 30, and 50 vol. % for: (a) $P = 100$ mN, (b) $P = 300$ mN (c) $P = 500$ mN.

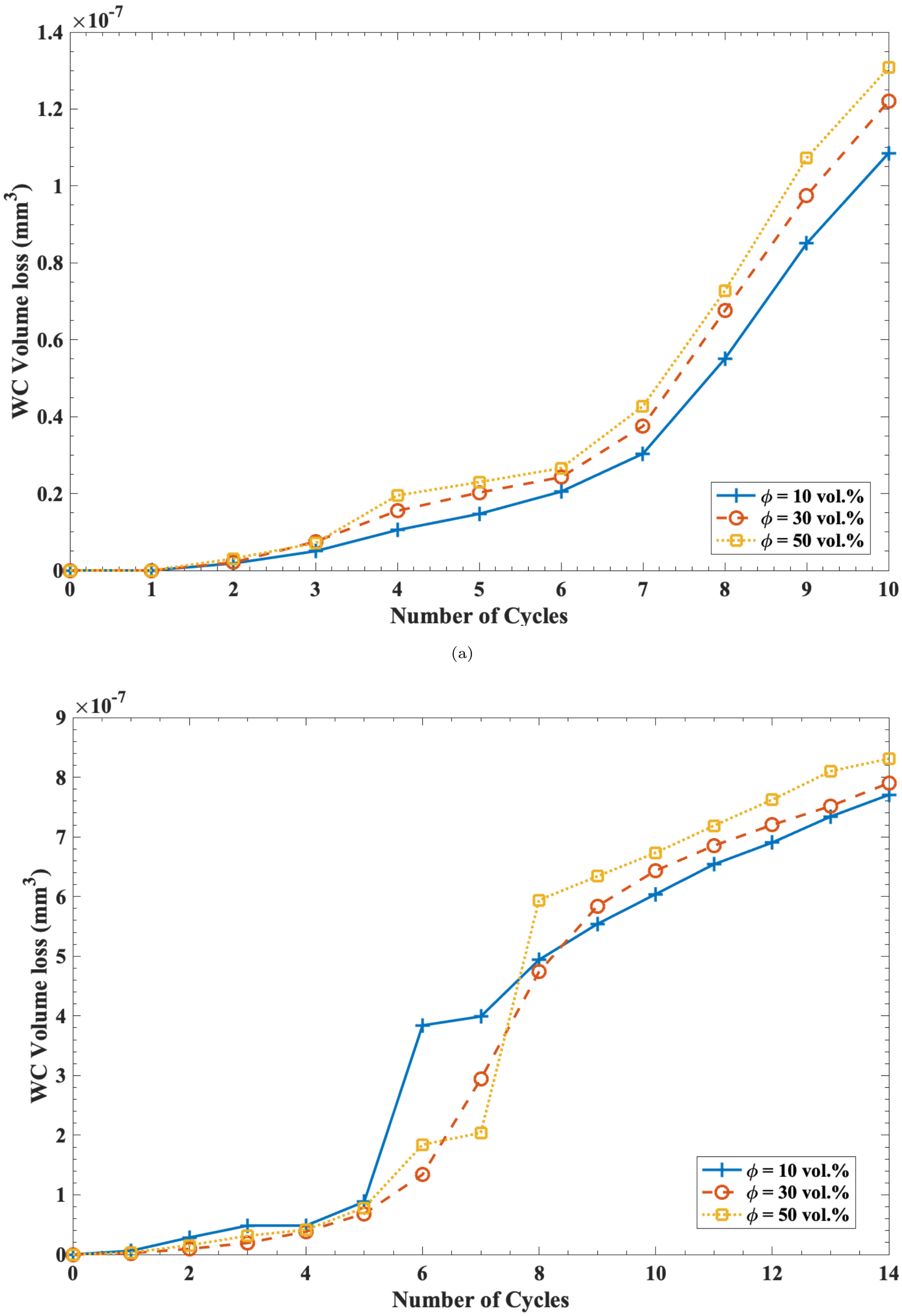

(a)

(b)

Figure 7: WC volume loss (mm^3) at 10, 30, and 50 vol % for: (a) $P = 300$ mN and (b) $P = 500$ mN.

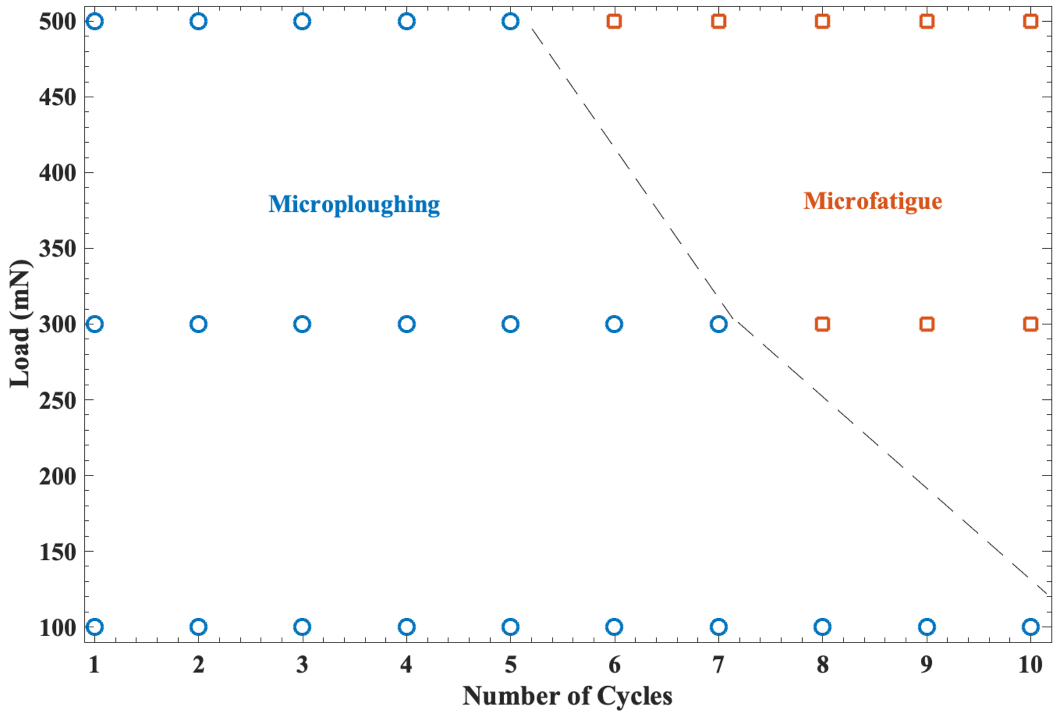

(a)

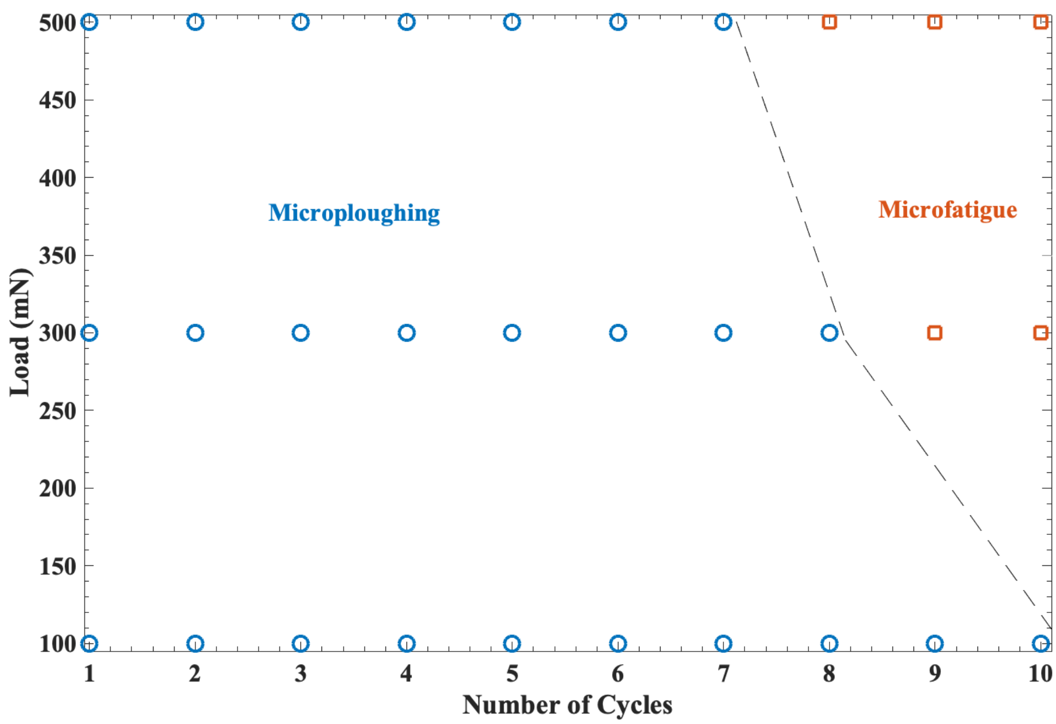

(b)

Figure 8: Wear mechanisms map (a) $\phi = 10$ vol.% and (b) $\phi = 50$ vol.%.

3.3. Prediction and correlation development of abrasive wear

A curve fitting approach, which was employed elsewhere [56, 57], was used to correlate independent variables (ϕ and P) with the response (W). To develop this correlation, MATLAB software was implemented. After checking different functional forms, the polynomial functional form was selected for this equation due to its accuracy in predicting the response (R^2=0.93). The correlation obtained using this approach can be described as:

$$W = -0.0004438 + 0.0001885 \times 10^{-9} P^{0.3} - 0.0001267 \times 10^{-6} \phi^{0.2} \tag{17}$$

Note the correlation is valid in the upper and lower limits of the variables used in this study. A graphical visualization of the correlation developed in Eq. (18) to predict the wear rate is illustrated in Fig. 9. Here, it was found that the relationship between the wear rate, load, and WC volume fraction is not linear, which indicates the role of different mechanisms and high nonlinearity of the problem, which was also reported elsewhere [58, 59]. The proposed model shows that the role of load is more significant than volume fraction of reinforcing particles and the role of volume fraction of reinforcing particles is less pronounced at lower loads than higher loads. While not explicitly studied in a systematic way in the literature, these observations are consistent with studies by Xia *et al.,* [54] and Idusuyi and Olayinka [60].

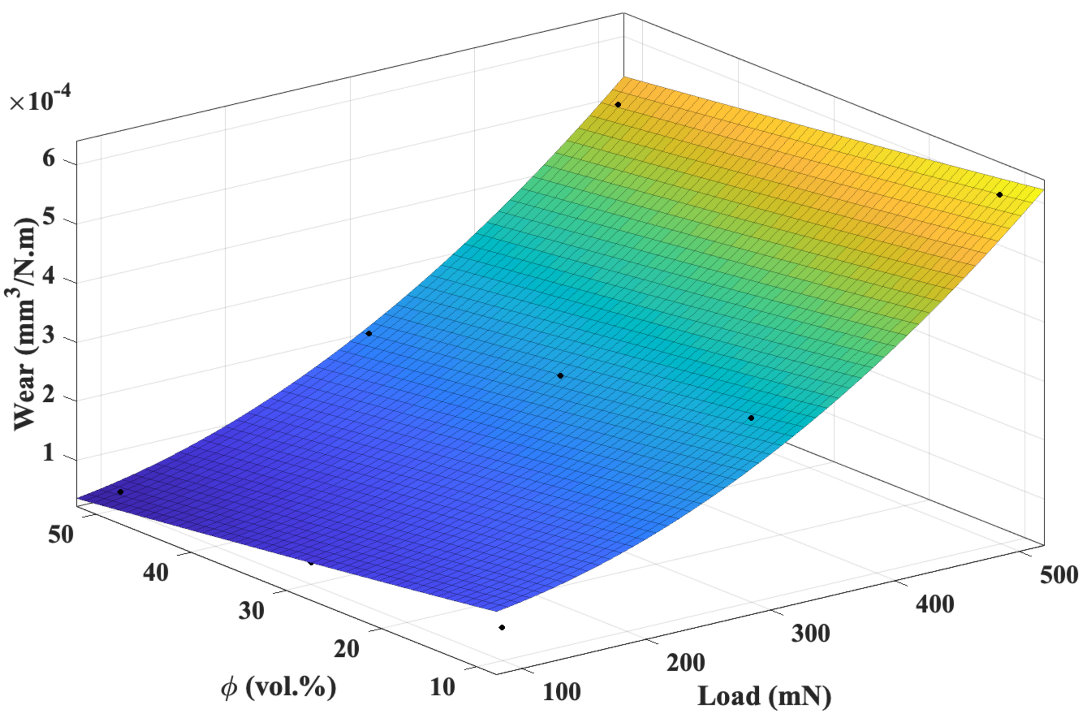

Figure 9: Prediction of wear rate variations at different loads and WC particles volume fractions.

4. Conclusion

In summary, the present work computationally evaluated the effects of applied load and WC particle volume concentration on the abrasive wear rate and material removal mechanisms in WC-Ni composite coatings under subcritical cyclic abrasive loadings. Results indicates that the load was better distributed in the composite with higher particles volume fraction. As a result, the wear rate was reduced with increasing the volume fraction of the WC particles when the load was 300 mN and lower. Removal of particles and earlier domination of microfatigue resulted in lower wear rates for the 30 vol.% of WC at the load of 500 mN, demonstrating the interplay between the material and loading parameters. The material removal mechanisms changed with increasing the number of cycles and volume fraction of the WC particle, as has been observed before in the literature [28]. Specifically, increasing the volume fraction of the reinforcing particles resulted in the onset of microfatigue for later cycles. This could be a reason for higher wear resistance of the material with a WC volume fraction of 50 vol.% when compared with the volume fraction of 10 vol.%. To clearly demonstrate the material removal mechanisms, wear mechanism maps were developed. It was shown that microploughing was the dominant material removal mechanism at early cycles regardless of the load and the volume fraction of the reinforcing particles, while microfatigue became more dominant at later cycles depending on the load and the volume fraction of reinforcing particles. To predict the wear rate of WC-Ni composite coatings and to better understand the relationship between the wear rate, load, and the volume fraction of reinforcing particles, a correlation was developed. Altogether, these results help better understand the relationship between different parameters (i.e., P, ϕ, and W) that govern material removal mechanisms and transitional behaviors under subcritical cyclic loading.

5. Acknowledgements

The authors acknowledge funding support from InnoTech Alberta, MITACS, the Natural Science and Engineering Research Council of Canada, the Canada Foundation for Innovation, and the Province of Alberta Ministry of Jobs, Economy, and Innovation. The authors also acknowledge Compute Canada for computing resources.

References

[1] N. Melendez, V. Narulkar, G. Fisher, A. McDonald, Effect of reinforcing particles on the wear rate of low-pressure cold-sprayed wc-based mmc coatings, Wear 306 (1) (2013) 185–195, 4th UK-China Tribology. doi:https://doi.org/10.1016/j.wear.2013.08.006.
URL https://www.sciencedirect.com/science/article/pii/S0043164813004596

[2] I. Ibrahim, F. Mohamed, E. Lavernia, Particulate reinforced metal matrix composites—a review, Journal of materials science 26 (5) (1991) 1137–1156.

[3] F. Rashed, T. Mahmoud, Prediction of wear behaviour of a356/sicp mmcs using neural networks, Tribology International 42 (5) (2009) 642–648. doi:https://doi.org/10.1016/j.triboint.2008.08.010.
URL https://www.sciencedirect.com/science/article/pii/S0301679X08001989

[4] Y. Li, X. Ge, H. Wang, Y. Hu, F. Ning, W. Cong, C. Ren, Study of material removal mechanisms in grinding of c/sic composites via single-abrasive scratch tests, Ceramics International 45 (4) (2019) 4729–4738. doi:https://doi.org/10.1016/j.ceramint.2018.11.165.
URL https://www.sciencedirect.com/science/article/pii/S0272884218332838

[5] S. Huang, D. Sun, W. Wang, H. Xu, Microstructures and properties of in-situ tic particles reinforced ni-based composite coatings prepared by plasma spray welding, Ceramics International 41 (9, Part B) (2015) 12202–12210. doi:https://doi.org/10.1016/j.ceramint.2015.06.041.
URL https://www.sciencedirect.com/science/article/pii/S0272884215011578

[6] A. Nieto, H. Yang, L. Jiang, J. M. Schoenung, Reinforcement size effects on the abrasive wear of boron carbide reinforced aluminum composites, Wear 390-391 (2017) 228–235. doi:https://doi.org/10.1016/j.wear.2017.08.002.
URL https://www.sciencedirect.com/science/article/pii/S0043164817305161

[7] W. Fu, Q.-Y. Chen, C. Yang, D.-L. Yi, H.-L. Yao, H.-T. Wang, G.-C. Ji, F. Wang, Microstructure and properties of high velocity oxygen fuel sprayed (wc-co)-ni coatings, Ceramics International 46 (10, Part A) (2020) 14940–14948. doi:https://doi.org/10.1016/j.ceramint.2020.03.021.
URL https://www.sciencedirect.com/science/article/pii/S0272884220306398

[8] Y. T. R. Lee, H. Ashrafizadeh, G. Fisher, A. McDonald, Effect of type of reinforcing particles on the deposition efficiency and wear resistance of low-pressure cold-sprayed metal matrix composite coatings, Surface and Coatings Technology 324 (2017) 190–200. doi:https://doi.org/10.1016/j.surfcoat.2017.05.057.
URL https://www.sciencedirect.com/science/article/pii/S0257897217305364

[9] M. Sabzi, S. M. Dezfuli, S. Mirsaeedghazi, The effect of pulse-reverse electroplating bath temperature on the wear/corrosion response of ni-co tungsten carbide nanocomposite coating during layer deposition, Ceramics International 44 (16) (2018) 19492–19504. doi:https://doi.org/10.1016/j.ceramint.2018.07.189.
URL https://www.sciencedirect.com/science/article/pii/S0272884218319291

[10] H. Vasudev, L. Thakur, H. Singh, A review on tribo-corrosion of coatings in glass manufacturing industry and performance of coating techniques against high temperature corrosion and wear, i-Manager's Journal on Material Science 5 (3) (2017) 38.

[11] L. N. Moskowitz, Application of hvof thermal spraying to solve corrosion problems in the petroleum industry—an industrial note, Journal of Thermal Spray Technology 2 (1) (1993) 21–29. doi:10.1007/BF02647419.
URL https://doi.org/10.1007/BF02647419

[12] A. Souza Oliveira Pimentel, W. Luiz Guesser, W. J. Rodrigues Custódio da Silva, P. Dolabella Portella, M. Woydt, J. Burbank, Abrasive wear behavior of austempered ductile iron with niobium additions, Wear 440-441 (2019) 203065. doi:https://doi.org/10.1016/j.wear.2019.203065.
URL https://www.sciencedirect.com/science/article/pii/S004316481930852X

[13] O. Zambrano, Y. Aguilar, J. Valdés, S. Rodríguez, J. Coronado, Effect of normal load on abrasive wear resistance and wear micromechanisms in femnalc alloy and other austenitic steels, Wear 348-349 (2016) 61–68. doi:https://doi.org/10.1016/j.wear.2015.11.019.
URL https://www.sciencedirect.com/science/article/pii/S0043164815004950

[14] M. Ben Tkaya, H. Zahouani, S. Mezlini, P. Kapsa, M. Zidi, A. Dogui, The effect of damage in the numerical simulation of a scratch test, Wear 263 (7) (2007) 1533–1539, 16th International Conference on Wear of Materials. doi:https://doi.org/10.1016/j.wear.2007.01.083.
URL https://www.sciencedirect.com/science/article/pii/S0043164807003900

[15] H. Li, Y. Xie, K. Li, L. Huang, S. Huang, B. Zhao, X. Zheng, Microstructure and wear behavior of graphene nanosheets-reinforced zirconia coating, Ceramics International 40 (8, Part B) (2014) 12821–12829. doi:https://doi.org/10.1016/j.ceramint.2014.04.136.
URL https://www.sciencedirect.com/science/article/pii/S0272884214006919

[16] W. Shi, H. Dong, T. Bell, Tribological behaviour and microscopic wear mechanisms of uhmwpe sliding against thermal oxidation-treated ti6al4v, Materials Science and Engineering: A 291 (1) (2000) 27–36. doi:https://doi.org/10.1016/S0921-5093(00)00972-2.
URL https://www.sciencedirect.com/science/article/pii/S0921509300009722

[17] I. Hutchings, P. Shipway, Tribology: friction and wear of engineering materials, Butterworth-Heinemann, 2017.

[18] S. K. Sharma, B. V. M. Kumar, Y.-W. Kim, Effect of wc addition on sliding wear behavior of sic ceramics, Ceramics International 41 (3) (2015) 3427–3437.

[19] M. Varga, S. Leroch, H. Rojacz, M. R. Ripoll, Study of wear mechanisms at high temperature scratch testing, Wear 388-389 (2017) 112–118, nORDTRIB 2016: The 17th Nordic Symposium on Tribology. doi:https://doi.org/10.1016/j.wear.2017.04.027.
URL https://www.sciencedirect.com/science/article/pii/S0043164817307329

[20] Y. Du, H. Chen, G. Yang, B. Liu, Y. Gao, H. Luo, Effect of cobalt content on high-temperature tribological properties of tic-co coatings, Ceramics International 44 (12) (2018) 14186–14194.

[21] M. Parsazadeh, G. Fisher, A. McDonald, J. Hogan, Computational investigation of the effect of microstructure on the scratch resistance of tungsten-carbide nickel composite coatings, Wear 478-479 (2021) 203888. doi:https://doi.org/10.1016/j.wear.2021.203888.
URL https://www.sciencedirect.com/science/article/pii/S0043164821002775

[22] M. Woldman, E. V. D. Heide, T. Tinga, M. A. Masen, A finite element approach to modeling abrasive wear modes, Tribology Transactions 60 (4) (2017) 711–718. arXiv:https://doi.org/10.1080/10402004.2016.1206647, doi:10.1080/10402004.2016.1206647.
URL https://doi.org/10.1080/10402004.2016.1206647

[23] C. Lyphout, G. Bolelli, E. Smazalova, K. Sato, J. Yamada, Š. Houdková, L. Lusvarghi, T. Manfredini, Influence of hardmetal feedstock powder on the sliding wear and impact resistance of high velocity airfuel (hvaf) sprayed coatings, Wear 430-431 (2019) 340–354. doi:https://doi.org/10.1016/j.wear.2019.05.016.
URL https://www.sciencedirect.com/science/article/pii/S0043164818315345

[24] M. Woldman, E. Van Der Heide, T. Tinga, M. Masen, The influence of abrasive body dimensions on single asperity wear, Wear 301 (1) (2013) 76–81, wear of Materials 2013. doi:https://doi.org/10.1016/j.wear.2012.12.009.
URL https://www.sciencedirect.com/science/article/pii/S0043164812004371

[25] K. Holmberg, A. Laukkanen, A. Ghabchi, M. Rombouts, E. Turunen, R. Waudby, T. Suhonen, K. Valtonen, E. Sarlin, Computational modelling based wear resistance analysis of thick composite coatings, Tribology International 72 (2014) 13–30. doi:https://doi.org/10.1016/j.triboint.2013.12.001.
URL https://www.sciencedirect.com/science/article/pii/S0301679X13004040

[26] J. Hu, D. Li, R. Llewellyn, Computational investigation of microstructural effects on abrasive wear of composite materials, Wear 259 (1) (2005) 6–17, 15th International Conference on Wear of Materials. doi:https://doi.org/10.1016/j.wear.2005.02.017.
URL https://www.sciencedirect.com/science/article/pii/S0043164805001080

[27] J. Hu, D. Li, R. Llewellyn, Synergistic effects of microstructure and abrasion condition on abrasive wear of composites—a modeling study, Wear 263 (1-6) (2007) 218–227.

[28] K. Kato, Wear mode transitions, Scripta Metallurgica et Materialia 24 (5) (1990) 815–820. doi:https://doi.org/10.1016/0956-716X(90)90118-Z.
URL https://www.sciencedirect.com/science/article/pii/0956716X9090118Z

[29] H. Kitsunai, K. Kato, K. Hokkirigawa, H. Inoue, The transitions between microscopic wear modes during repeated sliding friction observed by a scanning electron microscope tribosystem, Wear 135 (2) (1990) 237–249. doi:https://doi.org/10.1016/0043-1648(90)90028-9.
URL https://www.sciencedirect.com/science/article/pii/0043164890900289

[30] S. Mezlini, P. Kapsa, J. Abry, C. Henon, J. Guillemenet, Effect of indenter geometry and relationship between abrasive wear and hardness in early stage of repetitive sliding, Wear 260 (4) (2006) 412–421. doi:https://doi.org/10.1016/j.wear.2005.02.106.
URL https://www.sciencedirect.com/science/article/pii/S004316480500222X

[31] S. Alidokht, P. Manimunda, P. Vo, S. Yue, R. Chromik, Cold spray deposition of a ni-wc composite coating and its dry sliding wear behavior, Surface and Coatings Technology 308 (2016) 424–434, the 43rd International Conference on Metallurgical Coatings and Thin Films. doi:https://doi.org/10.1016/j.surfcoat.2016.09.089.
URL https://www.sciencedirect.com/science/article/pii/S0257897216311008

[32] G. Fisher, T. Wolfe, K. Meszaros, The effects of carbide characteristics on the performance of tungsten carbide-based composite overlays, deposited by plasma-transferred arc welding, Journal of thermal spray technology 22 (5) (2013) 764–771.

[33] J. Bucaille, E. Felder, G. Hochstetter, Mechanical analysis of the scratch test on elastic and perfectly plastic materials with the three-dimensional finite element modeling, Wear 249 (5) (2001) 422–432. doi:https://doi.org/10.1016/S0043-1648(01)00538-5.
URL https://www.sciencedirect.com/science/article/pii/S0043164801005385

[34] D. Tabor, The hardness of solids, Reviews of Physics in Technology 1 (3) (1970) 145–179. doi:10.1088/0034-6683/1/3/i01.
URL https://doi.org/10.1088/0034-6683/1/3/i01

[35] K. Pondicherry, D. Rajaraman, T. Galle, S. Hertelé, D. Fauconnier, P. De Baets, Optimization and validation of a load-controlled numerical model for single asperity scratch, Tribology Letters 68 (1) (2020) 45. doi:10.1007/s11249-020-1283-3.
URL https://doi.org/10.1007/s11249-020-1283-3

[36] S. Mzali, F. Elwasli, A. Mkaddem, S. Mezlini, A micromechanical scratch model to investigate wear mechanisms in ud-gfrp composites, Mechanics & Industry 19 (3) (2018) 305.

[37] Z.-C. Feng, Y.-F. Liu, Y. Li, G.-B. Sun, Z. Zhang, C.-X. Shi, Microstructure and high temperature reciprocating sliding wear properties of mosi2/tic/γ-ni composite coating in-situ synthesized by co-axial powder feeding plasma transferred arc cladding, Tribology International 129 (2019) 82–91. doi:https://doi.org/10.1016/j.triboint.2018.08.008.
URL https://www.sciencedirect.com/science/article/pii/S0301679X18303967

[38] W. Gao, L. Wang, J. Coffey, F. Daver, Finite element simulation of scratch on polypropylene panels, Materials & Design 140 (2018) 400–408. doi:https://doi.org/10.1016/j.matdes.2017.12.018.
URL https://www.sciencedirect.com/science/article/pii/S0264127517311231

[39] C. Guo, J. Chen, J. Zhou, J. Zhao, L. Wang, Y. Yu, H. Zhou, Effects of wc–ni content on microstructure and wear resistance of laser cladding ni-based alloys coating, Surface and Coatings Technology 206 (8) (2012) 2064–2071. doi:https://doi.org/10.1016/j.surfcoat.2011.06.005.
URL https://www.sciencedirect.com/science/article/pii/S0257897211005901

[40] J. Rolland, H. W.-L. Berre, A. Saulot, Y. Berthier, Instrumentation of a contact with the finite element method and experimental coupling: The case of the swiss lever escapement mechanism, Tribology International 111 (2017) 176–183. doi:https://doi.org/10.1016/j.triboint.2017.03.012.
URL https://www.sciencedirect.com/science/article/pii/S0301679X17301299

[41] S. Pal, H. Haider, P. J. Laz, L. A. Knight, P. J. Rullkoetter, Probabilistic computational modeling of total knee replacement wear, Wear 264 (7) (2008) 701–707. doi:https://doi.org/10.1016/j.wear.2007.06.010.
URL https://www.sciencedirect.com/science/article/pii/S0043164807005753

[42] G. R. Johnson, W. H. Cook, Fracture characteristics of three metals subjected to various strains, strain rates, temperatures and pressures, Engineering Fracture Mechanics 21 (1) (1985) 31–48. doi:https://doi.org/10.1016/0013-7944(85)90052-9.
URL https://www.sciencedirect.com/science/article/pii/0013794485900529

[43] J. F. Moxnes, J. A. Teland, S. Skriudalen, S. M. Bergsrud, L. Sundem-Eriksen, H. Fykse, Development of material models for semi-brittle materials like tungsten carbide, 2010.

[44] T. Holmquist, G. Johnson, Response of boron carbide subjected to high-velocity impact, International Journal of Impact Engineering 35 (8) (2008) 742–752, twenty-fifth Anniversary Celebratory Issue Honouring Professor Norman Jones on his 70th Birthday. doi:https://doi.org/10.1016/j.ijimpeng.

2007.08.003.
URL https://www.sciencedirect.com/science/article/pii/S0734743X07001303

[45] T. J. Holmquist, D. W. Templeton, K. D. Bishnoi, Constitutive modeling of aluminum nitride for large strain, high-strain rate, and high-pressure applications, International Journal of Impact Engineering 25 (3) (2001) 211–231.

[46] G. R. Johnson, T. J. Holmquist, An improved computational constitutive model for brittle materials, in: AIP conference proceedings, Vol. 309, American Institute of Physics, 1994, pp. 981–984.

[47] Y. Xia, B. Guo, G. Cong, X. Zhang, G. Zeng, Numerical simulation of rock fragmentation induced by a single tbm disc cutter close to a side free surface, International Journal of Rock Mechanics and Mining Sciences 91 (2017) 40–48.

[48] R. Ghelichi, S. Bagherifard, M. Guagliano, M. Verani, Numerical simulation of cold spray coating, Surface and Coatings Technology 205 (23-24) (2011) 5294–5301.

[49] J. F. Moxnes, J. A. Teland, S. Skriudalen, S. M. Bergsrud, L. Sundem-Eriksen, H. Fykse, Development of material models for semi-brittle materials like tungsten carbide, Norwegian Defence Research Establishment (FFI) (2010).

[50] T. Holmquist, G. Johnson, W. Gooch, Modeling the 14.5 mm bs41 projectile for ballistic impact computations, in: S. Syngellakis, Projectile Impact: Modelling Techniques and Target Performance Assessment, WIT Press Southhampton, 2014, pp. 73–87.

[51] O. M. Alzouma, M.-A. Azman, D.-L. Yung, V. Fridrici, P. Kapsa, Influence of different reinforcing particles on the scratch resistance and microstructure of different wc–ni composites, Wear 352 (2016) 130–135.

[52] A. Tangena, P. Wijnhoven, The correlation between mechanical stresses and wear in a layered system, Wear 121 (1) (1988) 27–35. doi:https://doi.org/10.1016/0043-1648(88)90028-2.
URL https://www.sciencedirect.com/science/article/pii/0043164888900282

[53] K. Jia, T. Fischer, B. Gallois, Microstructure, hardness and toughness of nanostructured and conventional wc-co composites, Nanostructured Materials 10 (5) (1998) 875–891, selected Papers from the Conference on Microstructure and its Effects on Amorphous, Nanophase and Nanocrystalline Materials TMS Annual Meeting and Exposition. doi:https://doi.org/10.1016/S0965-9773(98)00123-8.
URL https://www.sciencedirect.com/science/article/pii/S0965977398001238

[54] J.-K. Xiao, L. Zhang, K.-C. Zhou, X.-P. Wang, Microscratch behavior of copper-graphite composites, Tribology International 57 (2013) 38–45. doi:https://doi.org/10.1016/j.triboint.2012.07.004.
URL https://www.sciencedirect.com/science/article/pii/S0301679X12002423

[55] K. Bonny, P. De Baets, J. Vleugels, S. Huang, B. Lauwers, Dry reciprocating sliding friction and wear response of wc–ni cemented carbides, Tribology Letters 31 (3) (2008) 199–209.

[56] G. Stachowiak, Numerical characterization of wear particles morphology and angularity of particles and surfaces, Tribology International 31 (1) (1998) 139–157. doi:https://doi.org/10.1016/S0301-679X(98)00016-4.
URL https://www.sciencedirect.com/science/article/pii/S0301679X98000164

[57] S. Wang, S. Khatir, M. Abdel Wahab, Proper orthogonal decomposition for the prediction of fretting wear characteristics, Tribology International 152 (2020) 106545. doi:https://doi.org/10.1016/j.triboint.2020.106545.
URL https://www.sciencedirect.com/science/article/pii/S0301679X20303777

[58] P. K. Padhi, A. Satapathy, Analysis of sliding wear characteristics of bfs filled composites using an experimental design approach integrated with ann, Tribology Transactions 56 (5) (2013) 789–796.

[59] P. R. Pati, Prediction and wear performance of red brick dust filled glass–epoxy composites using neural networks, International Journal of Plastics Technology 23 (2) (2019) 253–260.

[60] N. Idusuyi, J. I. Olayinka, Dry sliding wear characteristics of aluminium metal matrix composites: a brief overview, Journal of Materials Research and Technology 8 (3) (2019) 3338–3346. doi:https://doi.org/10.1016/j.jmrt.2019.04.017.
URL https://www.sciencedirect.com/science/article/pii/S2238785418310135

Declaration of interests

☒ The authors declare that they have no known competing financial interests or personal relationships that could have appeared to influence the work reported in this paper.

☐The authors declare the following financial interests/personal relationships which may be considered as potential competing interests:

UNIVERSITY OF ALBERTA

DEPARTMENT OF MECHANICAL ENGINEERING

5-08F Department of Mechanical Engineering
9211 - 116 Street NW
Edmonton, Alberta, Canada T6G 1H9
www.mece.engineering.ualberta.ca

November 24, 2021

Dr. P. Vincenzini

General Editor, Ceramics International

Re: Manuscript Submission

Dear Dr. P. Vincenzini

We are pleased to submit a research paper entitled, "computational modelling of the effect of microstructure on the abrasive wear resistance of tungsten-carbide nickel composite coatings under sub-critical cyclic impact loading". In experiments, controlling input factors, particularly intrinsic factors, affecting the wear rate is difficult. To date, no studies have numerically evaluated the effects of external and intrinsic factors on the wear resistance of metal-matrix composites (MMC) coatings and overlays for multi-cycle loading. Also, no model has been developed to predict the wear rate of WC-Ni composite coatings. Simulating wear rate of MMC coatings under cyclic loading helps better understand the changes in material removal mechanisms, as the material removal mechanisms change with increasing the number of cycles. Thus, this paper aims to: (1) numerically analyze the effect of both external and intrinsic factors on the wear rate and material removal mechanisms of WC-Ni composite coatings under cyclic loading using parallelized computing approach, and (2) develop a model to predict the wear rate of the composite coating and evaluate the relationships of different factors.

To accomplish this, a finite element (FE) model was developed to simulate the wear rate in WC-Ni composite coatings with consideration for relevant material and damage models. The FE model was validated with the experimental studies published earlier. Then, wear rate and material removal mechanisms were analyzed at each cycle. Eventually, a model was developed to predict the relationship of different factor in WC-Ni composite coatings.

If any additional material is needed, please contact me.

Thank you for your consideration.

Sincerely,

Mohammad Parsazadeh, Ph.D,
Postdoctoral Fellow
Department of Mechanical Engineering
University of Alberta